MATERIALS CHEMISTRY
FRONTIERS

REVIEW

View Article Online
View Journal | View Issue

Cite this: *Mater. Chem. Front.*, 2024, **8**, 681

Self-assembled molecules as selective contacts for efficient and stable perovskite solar cells

Wenhui Li, *[a] Eugenia Martínez-Ferrero [a] and Emilio Palomares *[ab]

Received 18th September 2023,
Accepted 9th November 2023

DOI: 10.1039/d3qm01017a

rsc.li/frontiers-materials

The charge-selective contacts play a crucial role in the charge dynamics of solar cells. In the fast race to achieve higher power conversion efficiencies in perovskite-based devices, the avoidance of the detrimental effects due to interfacial charge recombination and/or poor charge extraction is the key to achieving high performance devices. The unique molecular structure of self-assembled molecules (SAMs) offers the possibility to tune the different parts of the molecule by precise design of its components to achieve desirable energy levels and molecular dipoles to facilitate the charge transfer. Therefore, the application of the SAMs as selective contacts emerges as a promising route to achieve high performance perovskite solar cells with the advantage of low material consumption, longer lifetimes and reduced interfacial non-radiative recombination. In this review, we summarize the recent literature about SAMs applied as selective hole or electron contacts. The objective of the present review is to unravel the open questions related to these molecules and propose our perspective about the development of SAMs for the development of cost-efficient and stable perovskite solar cells.

1. Introduction

Perovskite solar cells (PSCs) have attracted intensive attention due to their rapid development with currently certificated power conversion efficiency (PCE) of 26.0% comparable to silicon solar cells.[1–3] The improvement of PSCs is mainly attributed to the unique photoelectric properties of perovskite semiconductors such as large absorption coefficient,[4] long carrier lifetime,[5] low binding energy,[6] and tunable bandgap.[7] However, charge-selective contacts play a critical role as well regardless of the architecture of the device (shown in Fig. 1a) influencing the charge extraction and improving the device performance. Typically, for high-performance n–i–p devices, tin oxide (SnO_2) and (2,2′,7,7′-tetrakis(*N*,*N*′-di-*p*-methoxyphenylamine)-9,9′-spirobifluorene) (spiro-OMeTAD) are used as

[a] *Institute of Chemical Research of Catalonia (ICIQ-CERCA), Avda. Països Catalans, 16, 43007 Tarragona, Spain. E-mail: epalomares@iciq.es*
[b] *Catalan Institution for Research and Advanced Studies (ICREA), 08010 Barcelona, Spain*

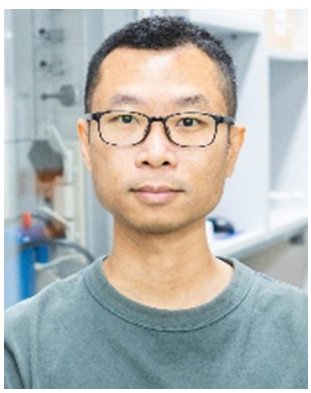

Wenhui Li

Dr Wenhui Li is currently a Postdoctoral Researcher in Institute of Chemical Research of Catalonia (ICIQ-CERCA) under the funding support of MSCA-COFUND I2: ICIQ Impulsion Programme. He received his PhD in materials science from the Institute of Process Engineering, Chinese Academy of Sciences in 2018. Then, he moved to the Southern University of Science and Technology, China as a Postdoctoral Fellow. His current research focuses on self-assembled molecules for highly efficient and stable perovskite solar cells.

Eugenia Martínez-Ferrero

Dr Eugenia Martinez-Ferrero holds a PhD in materials science from University of Valencia (Spain). She is currently scientific group coordinator in the group of Prof. Palomares at ICIQ, where she joined in 2021 after leading the optoelectronic device laboratory at Eurecat, a technological centre of Catalonia (Spain), for 10 years. Her background is on materials science and optoelectronic devices such as solar cells or light emitting devices. She is interested in establishing the relationship between the features of the materials and performance of the devices, in terms of efficiency and/or stability, a field where she has co-authored 76 publications,

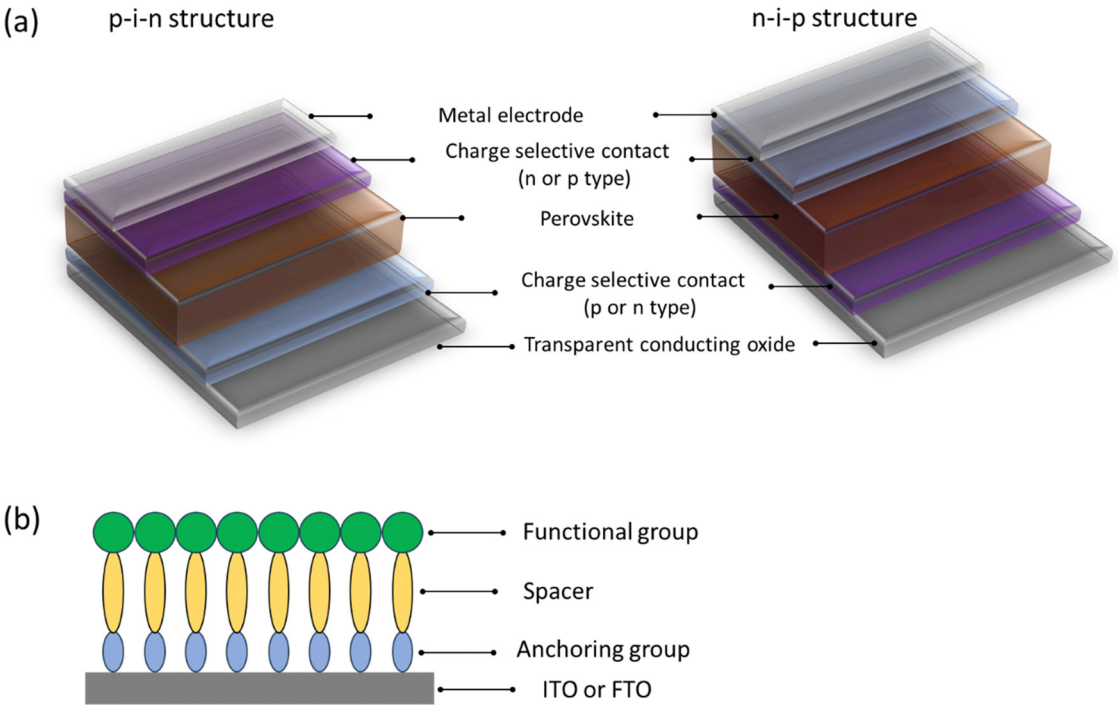

Fig. 1 (a) Configuration of typical p–i–n or n–i–p structure PSCs. (b) Schematic diagram of SAMs used as p-type or n-type charge selective contacts assembled onto ITO or FTO.

electron selective contact (ESC) and hole selective contact (HSC), respectively.[2,3,8] In turn, for high-performance p–i–n devices, poly[bis(4-phenyl)(2,5,6-trimethylphenyl)-amine] (PTAA) and [6,6]-phenyl-C61-butyric acid methyl ester ($PC_{61}BM$) or C_{60} fullerene are used as HSC and ESC, respectively.[9–12] Among them, the charge selective contacts deposited onto the substrate show a significant effect on the perovskite crystal growth, as well as the device stability.[13–15] However, despite the impressive performance of the PSCs, the commonly used charge selective contacts deposited onto the transparent conductive oxide are still subject to the high cost of the material, degradation under ambient conditions, instability under UV light and harsh processing, hindering the commercialization of PSCs.[16,17]

Self-assembled molecules (SAMs) have recently shown great potential as alternatives to the commonly used charge-selective contacts. Herein, we use the term of self-assembled molecules instead of the widely used self-assembled monolayers, owing to the difficulty of achieving a monolayer by the widely used current deposition process (*e.g.* spin coating). Additionally, such a charge-selective layer is formed by molecules. Thus, we select the term of self-assembled molecules to describe the abbreviation of SAMs precisely. SAMs can bond to the surface of the transparent conductive oxide chemically to the surface of the transparent conductive oxide (*e.g.* indium doped tin oxide – ITO – or fluorine-doped tin oxide – FTO) and spontaneously form ultrathin layers of a few nanometers. A SAM typically consists of three parts, namely an anchoring group, spacer (or bridge), and functional group (Fig. 1b). The combination of these three groups allows for the tuning of the molecule design to match the energy levels, charge mobility, and wettability to the properties of the perovskite solution dispersion.[15,18,19] SAMs form ordered arrays that, according to their structure, show a dipole moment able to modify the work function of the substrate, facilitating the charge extraction at the interfaces.[20,21] Furthermore, SAMs offer the possibility to passivate the buried surface of perovskite polycrystalline film and reduce the interfacial non-radiative recombination.[22] Finally, SAMs have the advantages of minimal parasitic absorption, low material consumption, and simplified fabrication which are convenient in the preparation of large-area and stable PSCs.

Emilio Palomares

Dr Emilio Palomares (ORCID 0000-0002-5092-9227) is ICREA Professor and group leader at ICIQ who became director of the Institute in 2020. He has extensive experience in the design and synthesis of materials for energy and the construction of third generation solar cells of different nature such as organic, quantum dot, dye sensitised or perovskite based. He was awarded in 2009 with an ERC Starting Grant and, in 2023 with an ERC Advanced Grant. Prof. Palomares has co-authored more than 200 peer-reviewed scientific papers on molecules and materials for energy-related devices.

This review summarizes these novel types of charge-selective contacts, including hole selective SAMs and electron selective SAMs used in p–i–n and n–i–p devices, respectively. After describing their structure and deposition methods, we have reviewed the application of the hole selective SAMs as a function of their anchoring groups, followed by the revision of the electron selective SAMs. We have also analyzed the interfacial charge transfer studies and discussed the influence of the molecular design and composition on the final efficiency of the devices.

2. The structure of SAMs

As mentioned above, the structure of the SAMs is made of three differentiated parts (Fig. 1b). Understanding the role of each part will help to rationally design molecules for high-performance devices.

2.1. Anchoring group

The anchoring groups are responsible for the interaction between the molecules and the substrate by chemical bonds, allowing the formation of films of molecules onto the substrate (typically ITO or FTO).[23] Various anchoring groups have been reported in the high-performance SAM-based PSCs, including carboxylic acid, phosphonic acid and cyanoacetic acid, among others.[19,24,25] The anchoring group acts as an internal molecular acceptor to balance the charge distribution within the molecule, modulating its molecular dipole and the energy levels of the molecule.

2.2. Spacer

The spacer (also called linker and bridge) is the backbone of the molecule connecting the anchoring group and the functional group. Both insulating alkyl groups and conjugated phenyl groups have been widely used in SAMs for high-performance devices. The alkyl spacers control the supramolecular

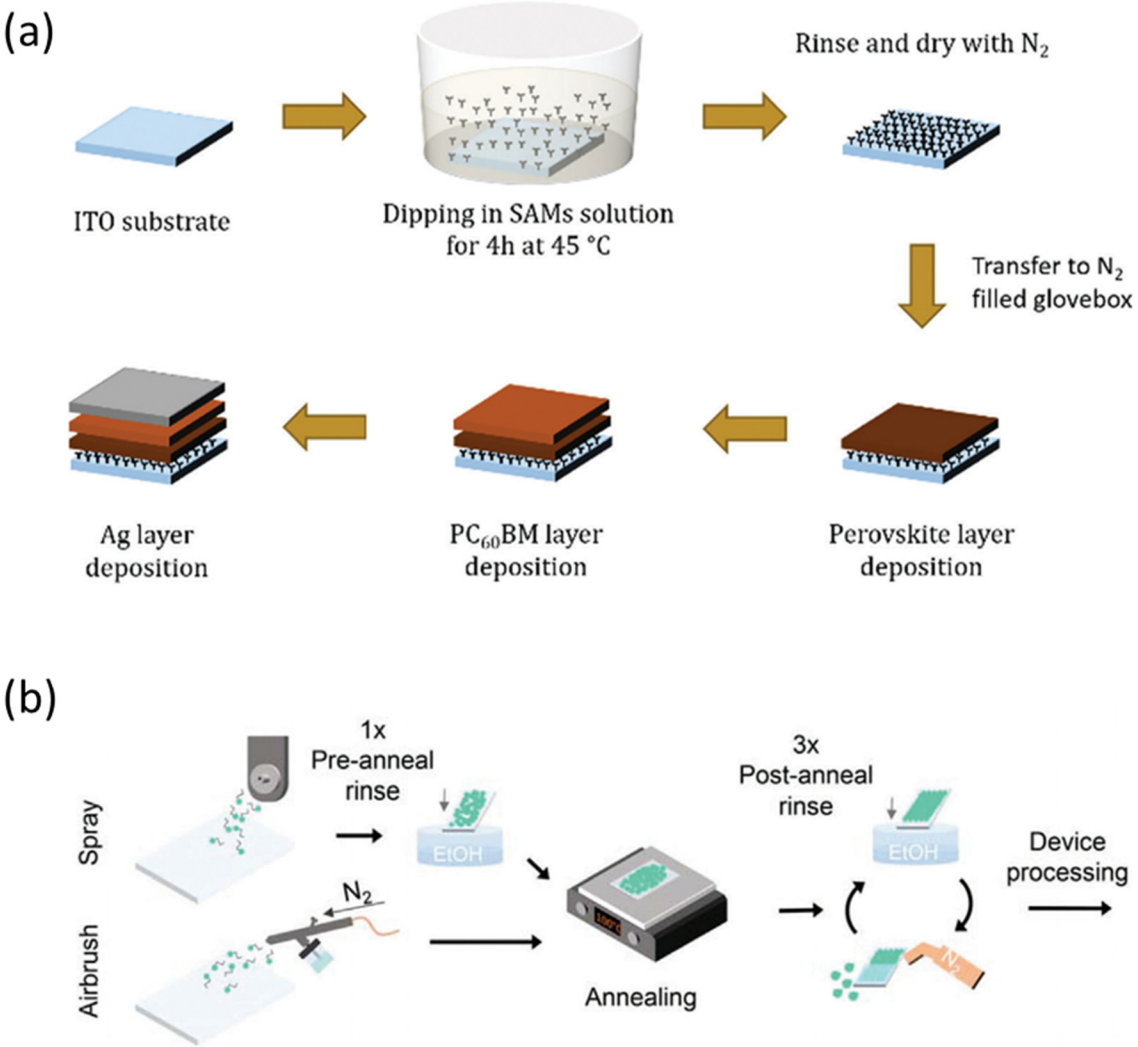

Fig. 2 (a) The dipping process to deposit SAMs onto ITO substrate. Reproduced with permission.[29] Copyright 2019, RSC. (b) The processes of spray- and airbrush-coated SAMs. Reproduced with permission.[30] Copyright 2022, Wiley.

structures *via* van der Waals interaction, therefore, the length of the alkyl chain influences these interactions between molecules, as well as the vertical alignment during the self-assembled process. Moreover, different chain lengths have a strong influence on the dipole moments and tunnelling lengths for interfacial charge transfer.[22,26] On the other hand, the conjugated phenyl spacer stabilizes the electron-rich functional group through effective charge delocalization and energy level modulation, which allows for electrochemically stable molecules.[25]

2.3. Functional group

The functional group, also called the terminal or head group, acts as a donor with electron-rich nature in hole-selective SAMs or as an electron acceptor in electron-selective SAMs. These groups are responsible for the interfacial reaction with perovskite enhancing the charge extraction, as well as influencing the molecular dipole that modulates the work function of the substrate.[27,28] The most used groups are carbazole and triphenylamine cores in the hole-selective SAMs, which are electron-rich structures that facilitate the hole extraction and transfer. In electron-selective SAMs, it is the fullerene core of the group of choice, being responsible for the electron extraction and transfer. On the other hand, the addition of functional groups such as methoxy or methyl groups can modulate the interfacial charge transfer rates and charge trapping.[19,26]

3. Deposition processes of SAMs

Various processes have been applied to deposit SAMs onto the ITO or FTO substrates to form selective electrodes, including solution process and vacuum deposition. In the next sections, there is a description of the most reported deposition techniques.

3.1. Dipping process

The substrates are immersed into a solution containing the molecule with a certain concentration, during a determined dipping time and temperature to allow the chemical adsorption and bonding of the SAM.[21,29] Subsequently, the substrates are rinsed with the same solvent to remove the unbonded

Table 1 The device performance based on hole selective SAMs with different anchoring groups

Anchoring groups	SAMs	Device configuration	J_{SC} (mA cm^{-2})	V_{OC} (V)	FF (%)	PCE (%)	Ref.
	TPA	ITO/TPA/$MAPbI_3$/$PC_{61}BM$/Ag	19.4	1.06	77	15.9	29
	MC-43	ITO/MC-43/$MAPbI_3$/$PC_{61}BM$/Ag	20.3	1.07	80	17.3	29
	EADR03	ITO/EADR03/$Cs_{0.05}FA_{0.79}MA_{0.16}Pb(I_{0.84}Br_{0.16})_3$/$C_{60}$/BCP/Cu	22.9	1.156	80	21.2	24
	EADR04	ITO/EADR04/$Cs_{0.05}FA_{0.79}MA_{0.16}Pb(I_{0.84}Br_{0.16})_3$/$C_{60}$/BCP/Cu	22.6	1.164	80	21.0	24
	RC24	ITO/RC24/$Cs_{0.05}FA_{0.79}MA_{0.16}Pb(I_{0.84}Br_{0.16})_3$/$C_{60}$/BCP/Cu	22.3	1.123	79	19.8	33
	RC25	ITO/RC25/$Cs_{0.05}FA_{0.79}MA_{0.16}Pb(I_{0.84}Br_{0.16})_3$/$C_{60}$/BCP/Cu	22.1	1.116	79	19.6	33
	RC34	ITO/RC34/$Cs_{0.05}FA_{0.79}MA_{0.16}Pb(I_{0.84}Br_{0.16})_3$/$C_{60}$/BCP/Cu	22.5	1.109	79	19.7	33
	Spiro-acid	ITO/Spiro-acid/$Cs_{0.05}FA_{0.81}MA_{0.14}Pb(I_{0.85}Br_{0.15})_3$/$C_{60}$/BCP/Ag	22.2	0.990	82.6	18.2	34
	TPT-C6	ITO/TPT-C6/$Cs_{0.05}MA_{0.12}FA_{0.83}Pb(I_{0.85}Br_{0.15})_3$/$C_{60}$/BCP/Ag	23.3	1.077	75.5	18.9	35
	V1036	ITO/V1036/$Cs_5(MA_{17}FA_{83})_{95}Pb(I_{83}Br_{17})_3$/$C_{60}$/BCP/Cu	21.2	1.041	79.3	17.5	19
	MeO-2PACz	ITO/MeO-2PACz/$Cs_5(MA_{17}FA_{83})_{95}Pb(I_{83}Br_{17})_3$/$C_{60}$/BCP/Cu	22.2	1.144	80.5	20.4	19
	2PACz	ITO/2PACz/$Cs_5(MA_{17}FA_{83})_{95}Pb(I_{83}Br_{17})_3$/$C_{60}$/BCP/Cu	21.9	1.188	80.2	20.8	19
	Me-4PACz	ITO/Me-4PACz/$Cs_5(MA_{23}FA_{77})_{95}Pb(I_{77}Br_{23})_3$/$C_{60}$/$SnO_2$/Ag	20.7	1.224	82.0	20.8	26
	Br-2EPT	FTO/Br-2EPT/$Cs_{0.05}(FA_{0.92}MA_{0.08})_{0.95}Pb(I_{0.92}Br_{0.08})_3$/$C_{60}$/BCP/Cu	25.11	1.09	82.0	22.4	36
	Br-2EPSe	FTO/Br-2EPT/$Cs_{0.05}(FA_{0.92}MA_{0.08})_{0.95}Pb(I_{0.92}Br_{0.08})_3$/$C_{60}$/BCP/Cu	24.49	1.12	82.86	22.73	37
	2BrPXZPA	ITO/2BrPXZPA/$Cs_{0.05}(FA_{0.85}MA_{0.15})_{0.95}Pb(I_{0.85}Br_{0.15})_3$/$PC_{61}BM$/BCP/Ag	23.59	1.19	81.7	22.9	38
	CbzNaph	ITO/CbzNaph/$Cs_{0.05}MA_{0.15}FA_{0.80}PbI_3$/$C_{60}$/BCP/Ag	24.69	1.17	83.4	24.1	27
	DC-PA + IAHA	ITO/DC-PA + IAHA/$Cs_{0.05}MA_{0.15}FA_{0.80}PbI_3$/$C_{60}$/BCP/Ag	24.66	1.16	82.5	23.6	39
	BCBBr-C4PA	ITO/BCBBr-C4PA/$FA_{0.8}Cs_{0.2}Pb(I_{0.6}Br_{0.4})_3$/$C_{60}$/ALD-$SnO_2$/Cu	17.54	1.286	82.6	18.6	40
	PPA	ITO/PPA/$Cs_{0.05}FA_{0.85}MA_{0.1}PbI_3$/PCBM/BCP/Ag	24.83	1.140	82.0	23.2	41
	PPAOMe	ITO/PPAOMe/$Cs_{0.05}FA_{0.85}MA_{0.1}PbI_3$/PCBM/BCP/Ag	24.70	1.10	79.2	21.5	41
	MPA-CPA	ITO/MPA-CPA/$Cs_{0.05}(FA_{0.95}MA_{0.05})_{0.95}Pb(I_{0.95}Br_{0.05})_3$/$C_{60}$/BCP/Ag	24.8	1.20	84.5	25.2	15
	1PATAT-C3	FTO/1PATAT-C3/$Cs_{0.05}FA_{0.80}MA_{0.15}PbI_{2.75}Br_{0.25}$/$EDAI_2$/$C_{60}$/BCP/Ag	24.0	1.06	82	21.1	42
	2PATAT-C3	FTO/2PATAT-C3/$Cs_{0.05}FA_{0.80}MA_{0.15}PbI_{2.75}Br_{0.25}$/$EDAI_2$/$C_{60}$/BCP/Ag	23.3	1.14	83	22.2	42
	3PATAT-C3	FTO/3PATAT-C3/$Cs_{0.05}FA_{0.80}MA_{0.15}PbI_{2.75}Br_{0.25}$/$EDAI_2$/$C_{60}$/BCP/Ag	24.5	1.13	83	23.0	42
	3PATAT-C4	FTO/3PATAT-C4/$Cs_{0.05}FA_{0.80}MA_{0.15}PbI_{2.75}Br_{0.25}$/$EDAI_2$/$C_{60}$/BCP/Ag	23.3	1.14	83	22.1	42
	DMAcPA	ITO/DMAcPA/$Cs_{0.05}(FA_{0.95}MA_{0.05})_{0.95}Pb(I_{0.95}Br_{0.05})_3$/$C_{60}$/BCP/Ag	25.69	1.187	84.73	25.9	43
	MPA-BT-CA	ITO/MPA-BT-CA/$(FA_{0.17}MA_{0.94}PbI_{3.01})_{0.95}(PbCl_2)_{0.05}$/$C_{60}$/BCP/Ag	22.25	1.13	84.8	21.2	44
	FMPA-BT-CA	ITO/FMPA-BT-CA/$(FA_{0.17}MA_{0.94}PbI_{3.11})_{0.95}(PbCl_2)_{0.05}$/$C_{60}$/BCP/Cu	23.33	1.151	83.3	22.4	45
	2FMPA-BT-CA	ITO/2FMPA-BT-CA/$(FA_{0.17}MA_{0.94}PbI_{3.11})_{0.95}(PbCl_2)_{0.05}$/$C_{60}$/BCP/Cu	22.81	1.143	83.1	21.7	45
	MPA-Ph-CA	ITO/MPA-Ph-CA/$Cs_{0.05}(FA_{0.92}MA_{0.08})_{0.95}Pb(I_{0.92}Br_{0.08})_3$/$C_{60}$/BCP/Ag	23.55	1.139	84.0	22.5	25
	Cz-CA	ITO/Cz-CA/$Cs_{0.05}(FA_{0.92}MA_{0.08})_{0.95}Pb(I_{0.92}Br_{0.08})_3$/$C_{60}$/BCP/Ag	~22.5	~1.03	~82	~19	25
	TPA-CA	ITO/TPA-CA/$Cs_{0.05}(FA_{0.92}MA_{0.08})_{0.95}Pb(I_{0.92}Br_{0.08})_3$/$C_{60}$/BCP/Ag	~21.8	~0.98	~77	16.5%	25
	MPA-CA	ITO/MPA-CA/$Cs_{0.05}(FA_{0.92}MA_{0.08})_{0.95}Pb(I_{0.92}Br_{0.08})_3$/$C_{60}$/BCP/Ag	~23	~1.03	~81	~19.5	25
	Cz-Ph-CA	ITO/Cz-Ph-CA/$Cs_{0.05}(FA_{0.92}MA_{0.08})_{0.95}Pb(I_{0.92}Br_{0.08})_3$/$C_{60}$/BCP/Ag	~23	~1.05	~82	~19.8	25
	TPA-Ph-CA	ITO/TPA-Ph-CA/$Cs_{0.05}(FA_{0.92}MA_{0.08})_{0.95}Pb(I_{0.92}Br_{0.08})_3$/$C_{60}$/BCP/Ag	~22.6	~1.08	~82.5	~20	25

J_{SC}: current density (mA cm^{-2}), V_{OC}: open-circuit voltage (V), FF: fill factor (%).

molecules to form the monolayer or ultrathin layer (Fig. 2a). A post-annealing step is usually necessary to strengthen the bonding between molecules and substrates.

3.2. Spin coating

Spin coating is a common method to deposit SAM layer, due to the simple, convenient, and rapid characteristics of the deposition process.[21] Similar to the dipping process, a post-annealing process is usually necessary in the spin coating method to strengthen the molecule bonding. However, the washing step is not required.

3.3. Slot-die coating, spray coating and airbrush coating

Slot-die coating is used to deposit SAMs in the fabrication of minimodules.[31] Moreover, spray coating and airbrush coating have also been applied as effective methods to deposit SAMs, following new protocols for rapid, widely accessible and high-throughput deposition, as shown in Fig. 2b.[30] These coating techniques have the potential to be scaled up for the preparation of large-area PSCs.

3.4. Vacuum deposition

In contrast to solution processes, the vacuum method to deposit SAMs avoids using solvents which may have a negative impact on the environment. The vacuum-based deposition methods can be incorporated into PV production lines for large-scale PSCs. Furthermore, evaporation facilitates conformal and uniform coatings on different types of substances, including flat and textured surfaces, which is expected to improve the process yield and reproducibility.[32]

4. Hole selective SAMs

SAMs can be used as hole-selective contacts due to their suitable energy level alignments with perovskite, facilitating the hole extraction and transfer, as well as blocking the electrons to avoid non-radiative recombination and current leakage. Rationally designed SAMs can modulate the molecular dipole and modify the work function of ITO or FTO. In this case, the work function can be aligned with the energy level of the photo-excited quasi-Fermi levels of the perovskite improving the photovoltage of the devices.

In this part, we will review the SAMs used as hole-selective contacts in high-performance PSCs according to the nature of the anchoring groups. Table 1 summarizes the performance of hole-selective SAM-based p–i–n devices.

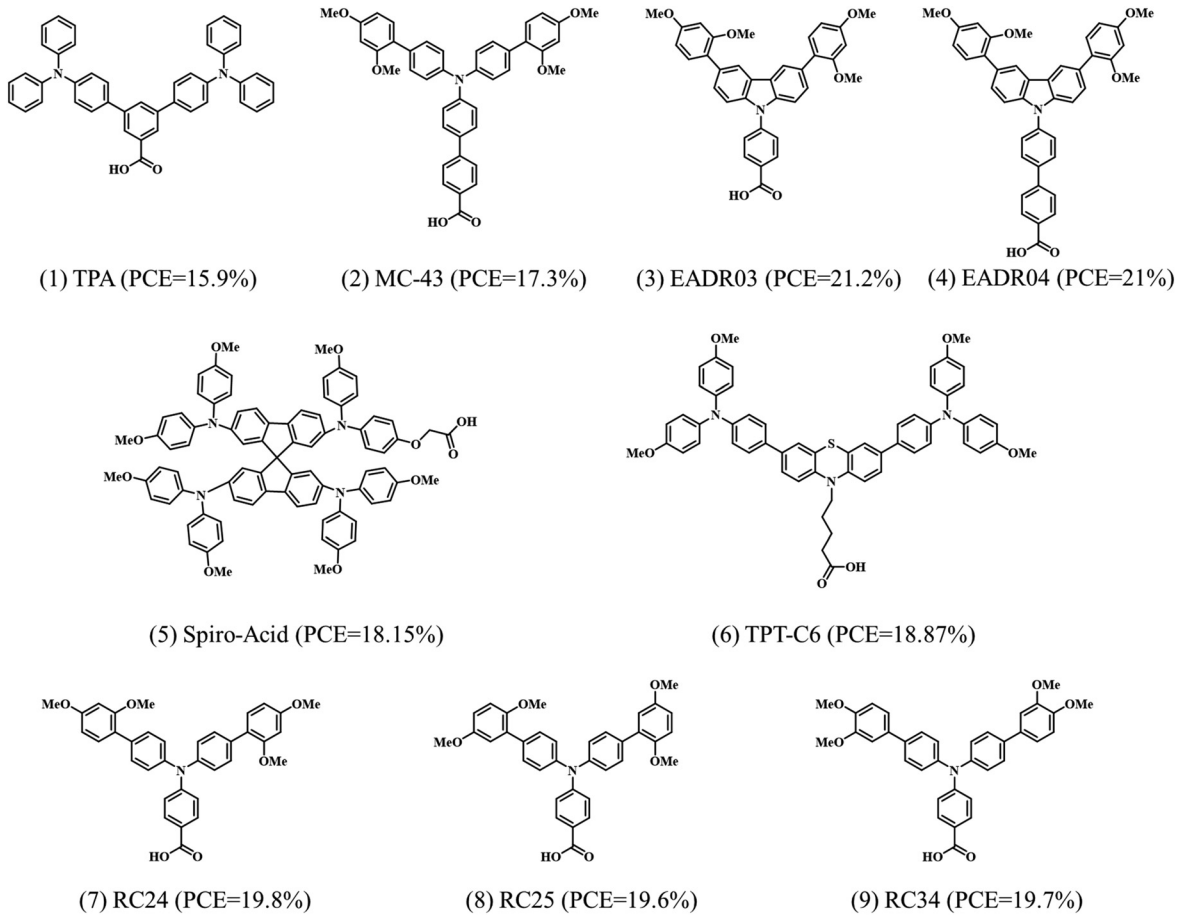

Fig. 3 Reported SAMs with carboxylic acid anchoring groups applied as hole selective contacts and the corresponding PCE achieved in the PSCs.

4.1. Carboxylic acid-based SAMs

Our group first reported carboxylic acid-based SAMs as hole-selective electrodes in p–i–n PSCs.[29] A summary of the reported SAMs containing carboxylic acid as the anchoring group is summarized in Fig. 3 together with the indication of the PCE.

The carboxylic acid anchors to the ITO surface either by mono- or bidentate binding modifying its work function.[46] Typically, monodentate bonds are formed by condensation of –OH groups of the SAM with surface hydroxyl groups of the ITO followed by the elimination of a water molecule to form a C–O–M bond. The bidentate binding takes place with a second condensation by transferring the hydrogen to the surface hydroxyl group and the subsequent release of a second water molecule.

The first reported results consisted of two carboxylic acid-based molecules, TPA and MC-43, that were directly assembled at the ITO electrode to modify the surface and enhance hole extraction in p–i–n PSCs.[29] The best device made with TPA showed a PCE of 15.9% with J_{SC} of 19.4 mA cm^{-2}, V_{OC} of 1.06 V and FF of 77%. Meanwhile, MC-43 SAM-based device showed a PCE of 17.3% with J_{SC} of 20.3 mA cm^{-2}, V_{OC} of 1.07 V and FF of 80% (Fig. 4a), among the highest efficiency at the time of publication. The improvement was ascribed to the suitable energy alignment of the MC-43 modified ITO with the perovskite, as well as the formation of homogeneous perovskite layers that enable good charge extraction, giving rise to the high FF and V_{OC} values. Later, the performance was further improved by two carbazole-based SAMs, EADR03 and EADR04 with carboxylic acid anchoring groups.[24] Stable efficiencies above 21% were obtained with V_{OC} up to 1.19 V for the triple cation perovskite of 1.63 eV bandgap. Remarkably, the devices retained 80% of their initial efficiency after 250 h, demonstrated by the tracking of the maximum power point (MPP) under AM 1.5G illumination at 85 °C, as shown in Fig. 4b. The excellent stability was ascribed to the delocalization of electrons on the phenyl moiety and the robustness in front of the UV light of the SAMs.

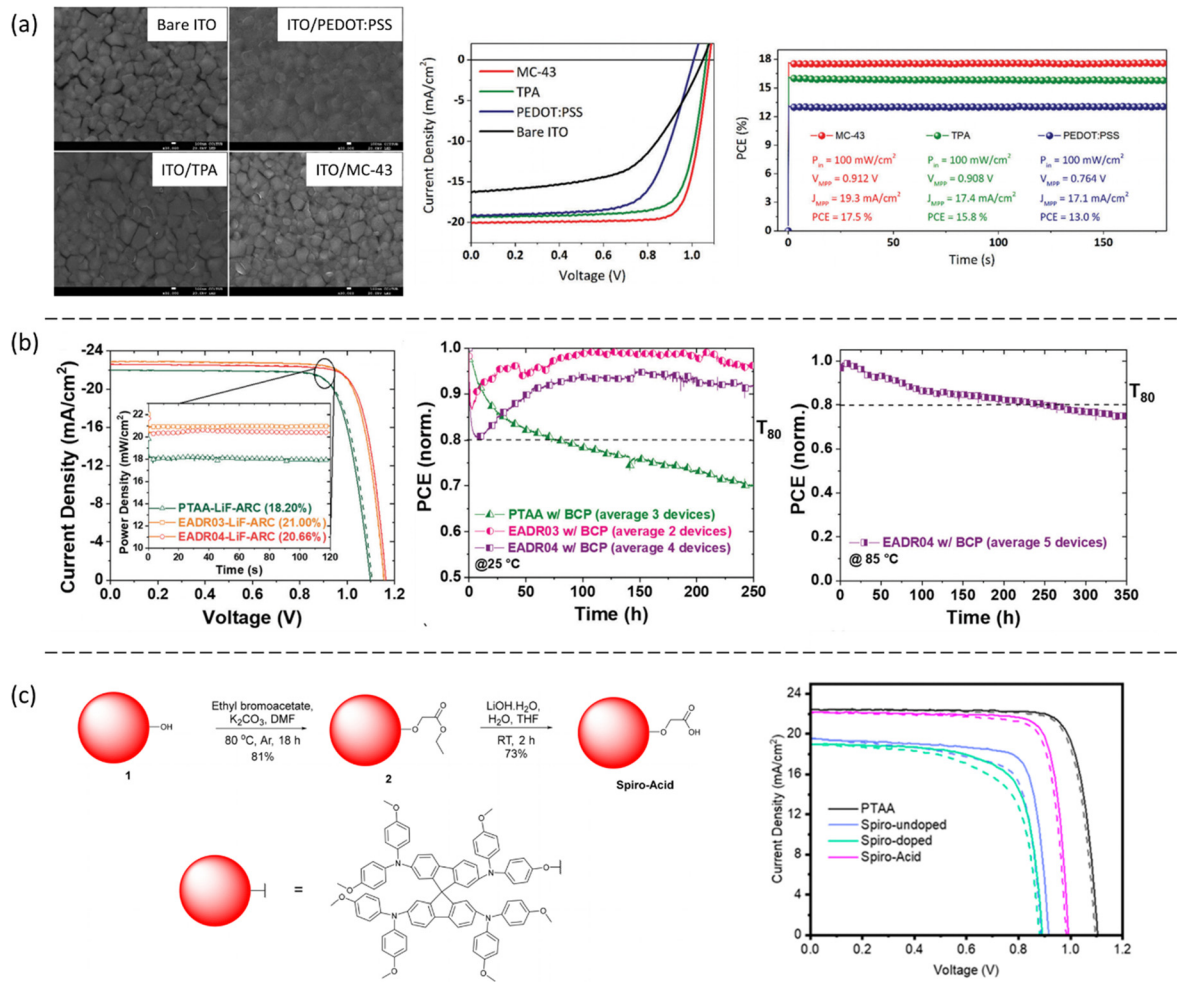

Fig. 4 (a) Morphology of the perovskite deposit onto the TPA and MC-43 SAM layer, and the corresponding device performance. Reproduced with permission.[29] Copyright 2019, RSC. (b) Device performance of EADR03 and EADR04 and their variation with time. Reproduced with permission.[24] Copyright 2021, RSC. (c) The synthesis process of spiro-acid SAM and the corresponding device performance. Reproduced with permission.[34] Copyright 2023, ACS.

Recently, our group modified the commercial and inexpensive unsublimed spiro-OMeTAD by introducing a carboxylic acid as an anchoring group, allowing the formation of the SAM layer onto ITO (Fig. 4c) by an easy-to-use methodology.[34]

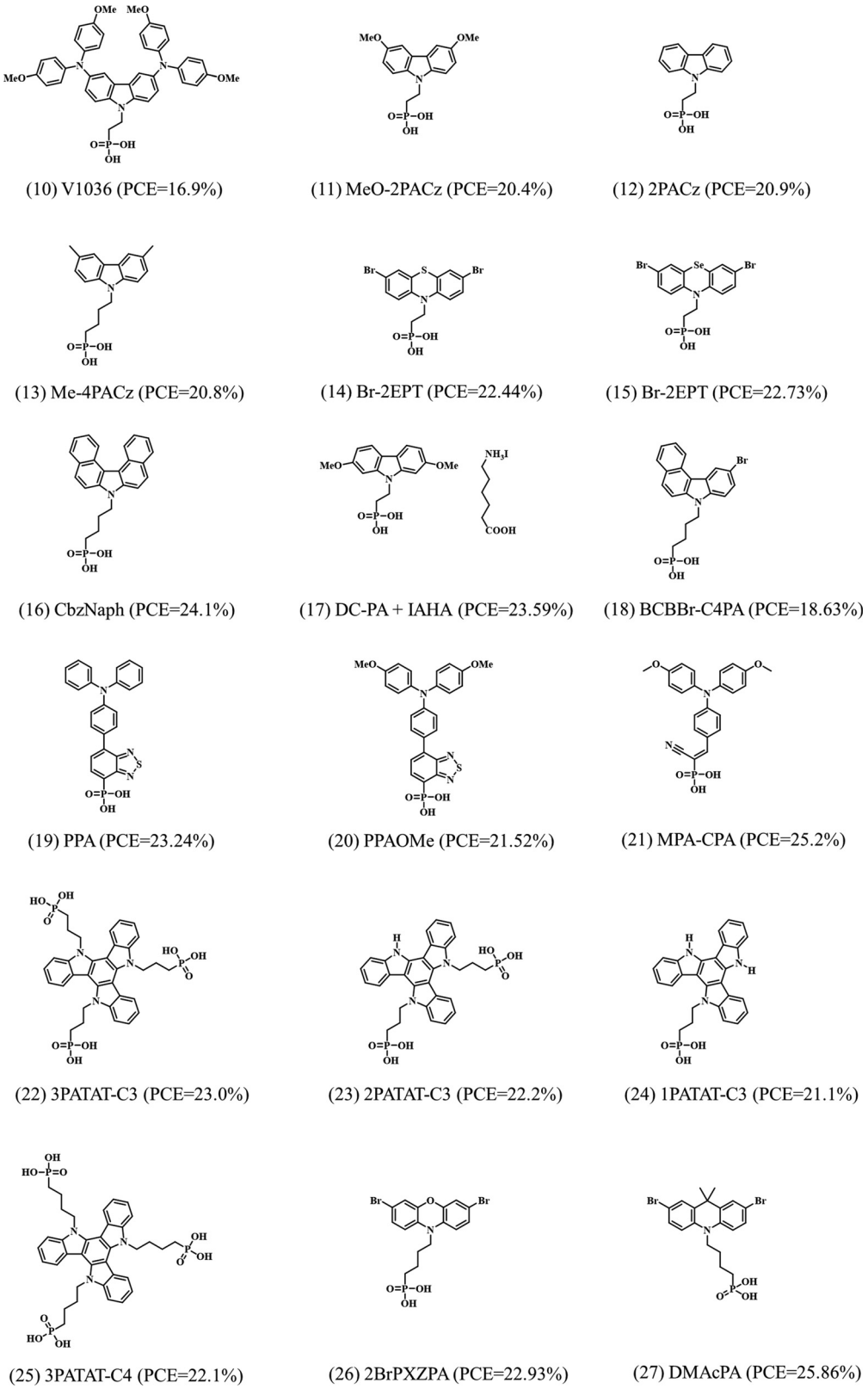

Fig. 5 Molecular structure of the reported SAMs with phosphonic acid as anchoring groups acting as hole selective contacts in PSCs and their corresponding PCE.

The device performance showed a best efficiency of 18.15% with ultralow energy loss, which is comparable to the PTAA-based PSCs, showing the highest efficiency among spiro-OMeTAD-based p–i–n PSCs. Significantly, the spiro-acid-based devices have a remarkable fill factor of over 82%, as well as excellent long-term stability under illumination, demonstrating the possibility to modify the commercial molecules as SAMs by simply introducing an anchoring group. In this case, the improved performance of the spiro-acid PSC compared to traditional spiro-OMeTAD PSC was due to the formation of an ultrathin layer combined with reduced charge transfer resistance.

4.2. Phosphonic acid-based SAMs

Getautis *et al.* first reported a SAM with phosphonic acid as an anchoring group, namely V1036, in 2018.[18] Later, the same group proposed a series of SAMs based on carbazole bodies with phosphonic acid anchoring groups, increasing the efficiency in single junction PSC up to 21%, which is comparable to record-efficiencies in the p–i–n architecture at that time, as shown in Fig. 6a.[19] Interestingly, the interfacial density of defects between the 2PACz SAM and perovskite decreases, as observed from the photoluminescence (PL) lifetime decay study, indicating that the bare carbazole is chemically compatible to the perovskite and able to form well-passivated surface. Tan *et al.* further proved that the defect passivation effect is ascribed to the chemical bonding between Pb and O from the phosphoryl of the 2PACz, which restores the six-coordinate local chemical environment for Pb.[47,48] More details will be discussed about interfacial charge transfer in the following part. Fig. 5 summarizes the SAMs with the phosphonic acid anchoring group and the corresponding device performance.

After the successful application of the 2PACz, several SAMs were synthesized by modifying this molecule with different aliphatic chain lengths (n), without the functional nPACz group or adding methyl substitution (Me-nPACz). The molecules were tested in combination with wide bandgap perovskites (1.68 eV) for single junction PSCs and in perovskite/silicon tandem cells (Fig. 6b). A PCE of 20.8% and a certified PCE of 29.15% were reported by using Me-4PACz SAM as the hole selective contact in the wide bandgap PSC and the perovskite/silicon tandem cell, respectively, ascribing the increase in efficiency to the fast hole extraction and minimized nonradiative recombination at the hole-selective interface.[26]

Hong *et al.* designed and synthesized a novel halogenated phenothiazine-based SAM (Br-2EPT) as hole selective contact in p–i–n PSCs.[36] In this molecule, the phenothiazine of the functional group contains electron-withdrawing bromide groups, an aliphatic chain acts as a linker and the phosphonic acid is the anchoring group. This combination allows for a better energetic alignment with the perovskite layer and superior electron-blocking ability. This molecule leads to a maximum PCE of over 22% with FF up to 82%. Remarkably, the Br-2EPT-based PSC showed good stability, retaining its initial efficiency during MPP tracking for over 100 h under AM 1.5G illumination in air without encapsulation. Similar functional groups were later added to SAMs by He *et al.*, named 2BrPXZPA, with bromine-substituted phenoxazine doped with an O atom as a functional

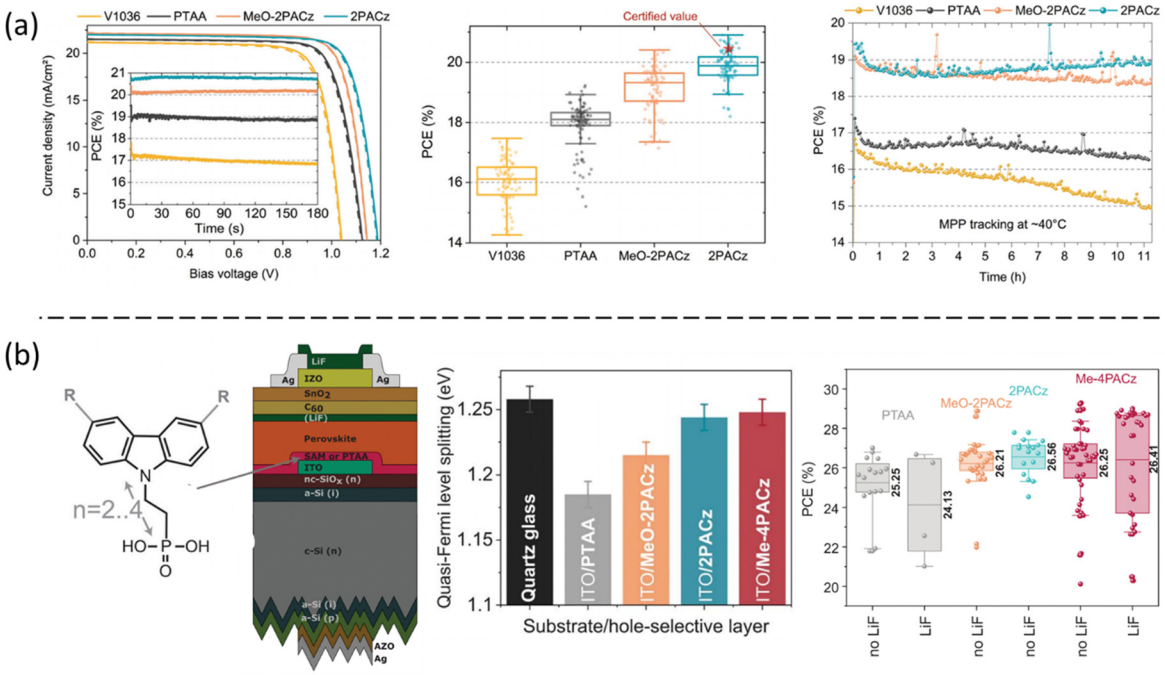

Fig. 6 (a) The device performance of carbazole-based SAMs with phosphonic acid anchoring group. Reproduced with permission.[19] Copyright 2019, RSC. (b) Structure of the perovskite/silicon tandem cell made with SAMs as hole selective contacts. Reproduced with permission.[26] Copyright 2020, AAAS.

group and a butyl chain as the spacer.[38] The phenoxazine group has strong electron-donating ability, allowing it to match energy levels with the perovskite decreasing the energy loss for 2BrPXZPA-based devices. The corresponding p–i–n PSC achieved a high PCE of 22.93% (certified 22.38%), as well as good stability retaining 97% of the initial efficiency after 600 h of MPP tracking under one sun continuous illumination.

Jen *et al.* designed two carbazole-based SAMs, CbzPh and CbzNaph, through asymmetric or helical π-expansion from the original 4PACz to improve the molecular dipole moment and strengthen the π–π interaction (Fig. 7a). The helical π-expanded CbzNaph has the largest dipole, forming densely packed and ordered monolayers that significantly improve the perovskite crystallization. Moreover, the monolayer effectively modulates the ITO work function that facilitates the interfacial charge transfer, allowing an excellent 24.1% efficiency and improved stability (Fig. 7b and c).[27] The same group later proposed a strategy to co-assemble molecules by combining a carbazole-based hole-selective SAM molecule (DC-PA) with an alkyl ammonium SAM (IAHA) as the second component in the hole-selective SAM matrix.[39] This combination gives rise to uniform and dense hole-selective films that avoid the leakage

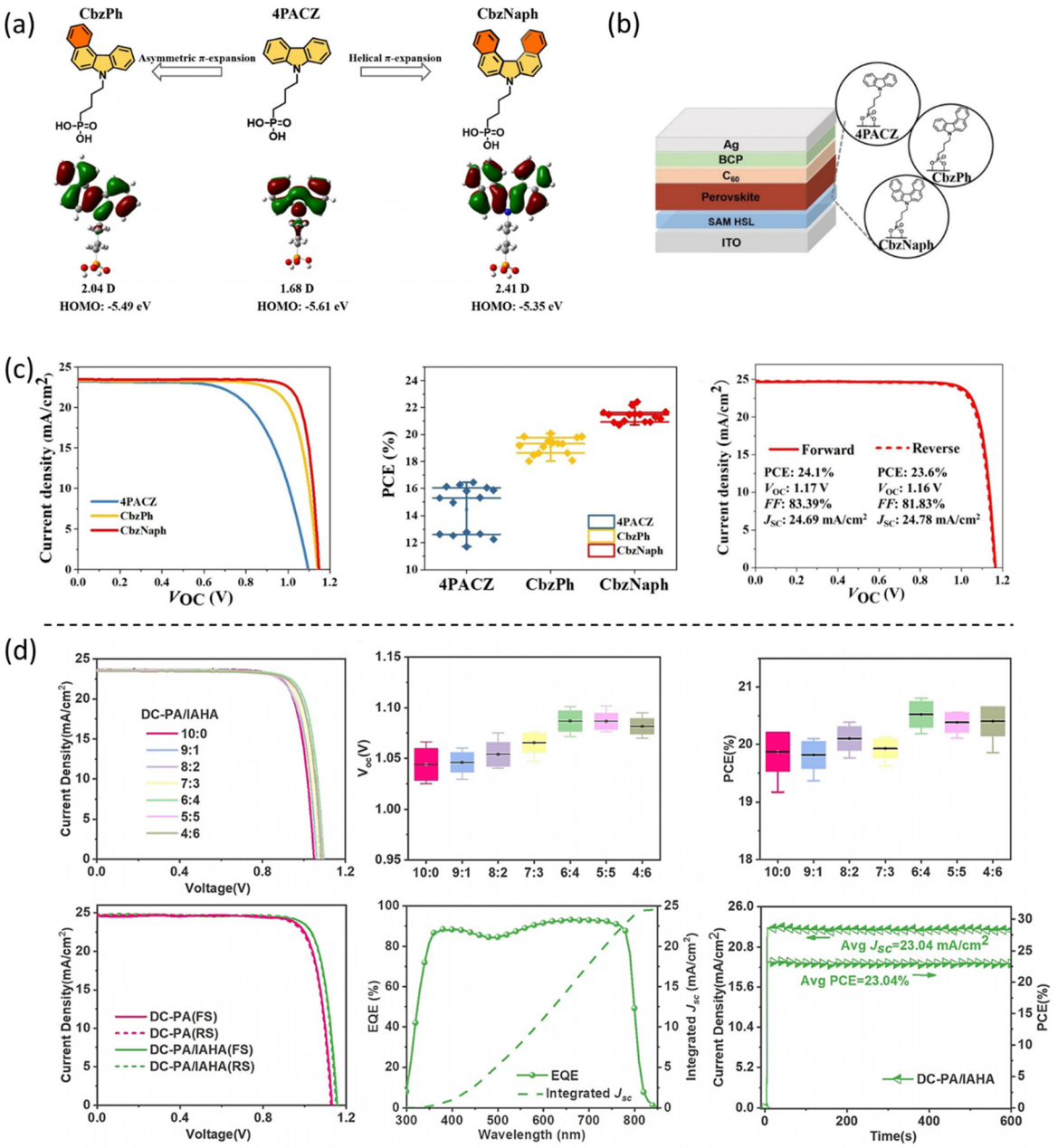

Fig. 7 (a) The π-expanded carbazole-based molecules and their calculated molecular dipole. (b) Device architecture of the CbzPh and CbzNaph-based p–i–n PSC and (c) their corresponding device performance. Reproduced with permission.[27] Copyright 2022, Wiley. (d) Device performance is based on the co-assembled DC-PA and IAHA monolayer substrates. Reproduced with permission.[38] Copyright 2022, Wiley.

current at the interface and the degradation of the device. The resulting p–i–n PSCs can reach a PCE of 23.59% with improved device stability (Fig. 7d). Wakamiya *et al.* also proposed SAMs with functionalized π-conjugated structures by introducing multiple phosphonic acids as anchoring groups (named 1PATAT-C3, 2PATAT-C3, 3PATAT-C3, and 3PATAT-C4).[42] Among them, the molecule with three phosphonic acids aligns face-on to the electrode surface. The preferred orientation of the π-core facilitates the hole extraction and results in the PCE up to 23.0%.

Tang *el al.* designed a new SAM called BCBBr-C4PA, exhibiting simultaneously improved solubility and large dipole moment by combining an asymmetric conjugation bone and bromination strategies in the molecular design.[40] The molecule is beneficial for the interfacial charge transfer in wide bandgap (E_g > 1.75 eV) PSCs. The target PSC has an impressive PCE of

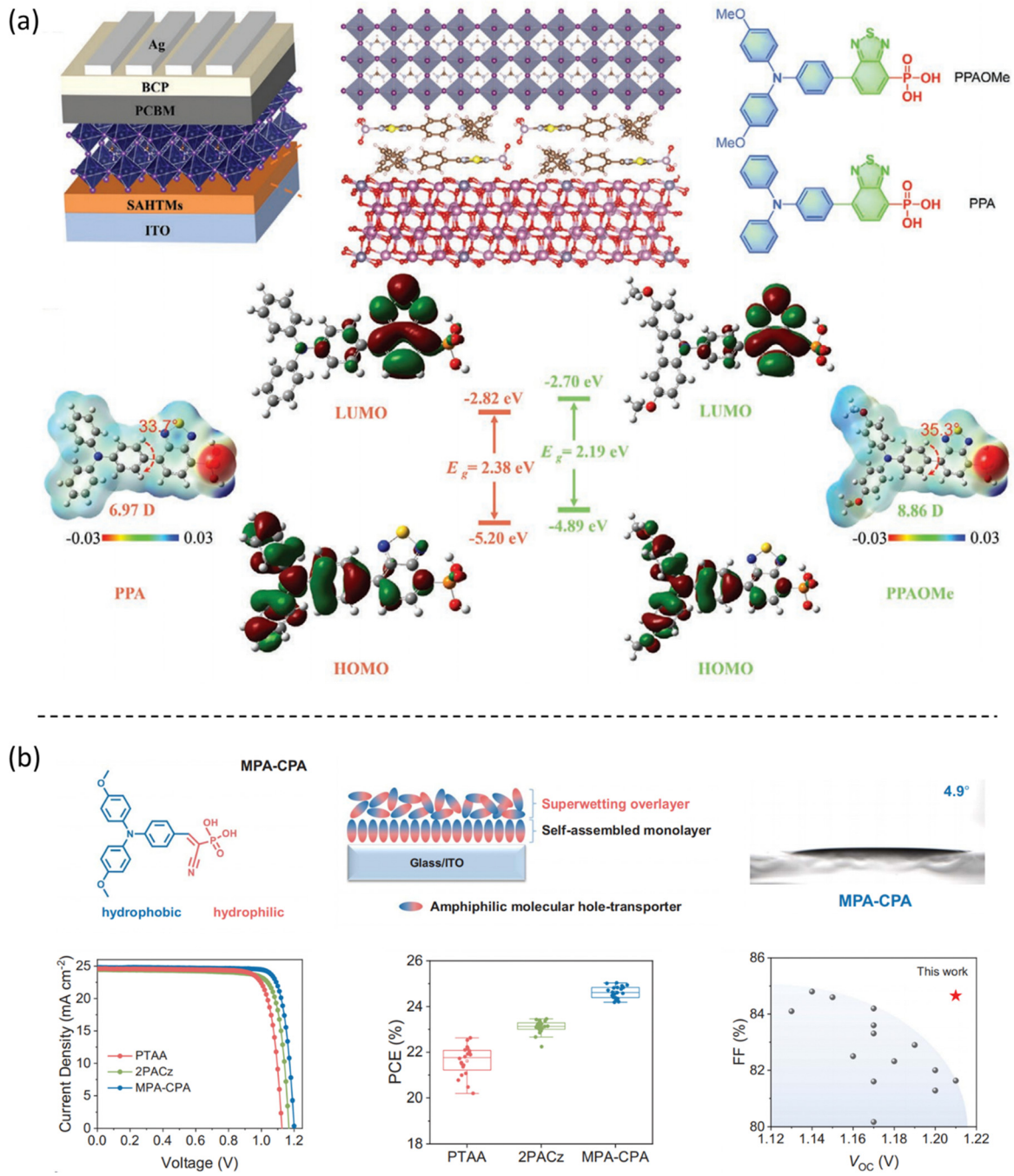

Fig. 8 (a) The molecular structures of PPA and PPAOMe and the corresponding calculated HOMO/LUMO levels. Reproduced with permission.[41] Copyright 2023, Wiley. (b) Schematic depiction of the bilayer stack of MPA-CPA molecules on an ITO–glass substrate and the corresponding device performance. Reproduced with permission.[15] Copyright 2023, AAAS.

18.63% with improved operation stability (over 90% PCE retention after 250 h continuous working), being one of the highest PCEs for wide bandgap PSCs. Li *et al.* designed multifunctional phosphonic acid-based SAM (PPA and PPAOMe) with the donor–acceptor subunit for hole transporting, realizing face-on π-stacking parallel to the ITO and allowing to grow high-quality perovskite films (Fig. 8a). The highly efficient p–i–n PSC was obtained with a best PCE of 23.24%.[41] Recently, Wu *et al.* modified the phosphonic acid anchoring group by adding a cyano group, forming a hydrophilic cyanovinyl phosphonic acid group.[15] The newly designed SAMs, called MPA-CPA, can form a bilayer stack consisting of a chemically anchored monolayer plus an unadsorbed, disordered overlayer (Fig. 8b). This special design results in a super wetting top surface that facilitates the deposition of the perovskite solution, particularly, in large substrates. The molecule also acts passivating defects reducing the interfacial non-radiative recombination loss and achieving a certified PCE of 25.4% with an open-circuit voltage of 1.21 V and a fill factor of 84.7%. Most recently, He *et al.* proposed the use as a dopant in the perovskite solution of a promising dimethylacridine-based molecule called DMAcPA.[43] The DMAcPA tunes the crystallinity of perovskite, and simultaneously, chelates with PbI_x that is extruded to the film bottom surface, tailoring the interface between perovskite and ITO. This has resulted in a record device efficiency of 25.86%. This work indicates that the phosphonic acid anchoring group has the function of bonding to ITO surface, and in addition and more importantly, of passivating the perovskite.

4.3. Cyanoacrylic acid-based SAMs

Fig. 9 summarizes the reported SAMs containing cyanoacrylic acid as an anchoring group and the corresponding device performance. The cyanoacrylic acid anchoring groups have been widely used in molecules for dye-sensitized solar cells,[49–51] since the D–A-type backbone was found to be beneficial for inducing intramolecular charge transfer. Such D–A-type structure is also useful in the hole-selective molecules for increasing the hole extraction and reducing exciton recombination in PSCs.

Moreover, the cyanoacrylic acid can be used to passivate perovskite defects owing to their Lewis base nature to coordinate Pb^{2+} defects.[52] Based on these concepts, Guo *et al.* designed a new SAM, called MPA-BT-CA, involving an anchoring group-assisted D–A-type structure with 4-methoxy-*N*-(4-methoxyphenyl)-*N*-phenylaniline (MPA) as the donor unit,

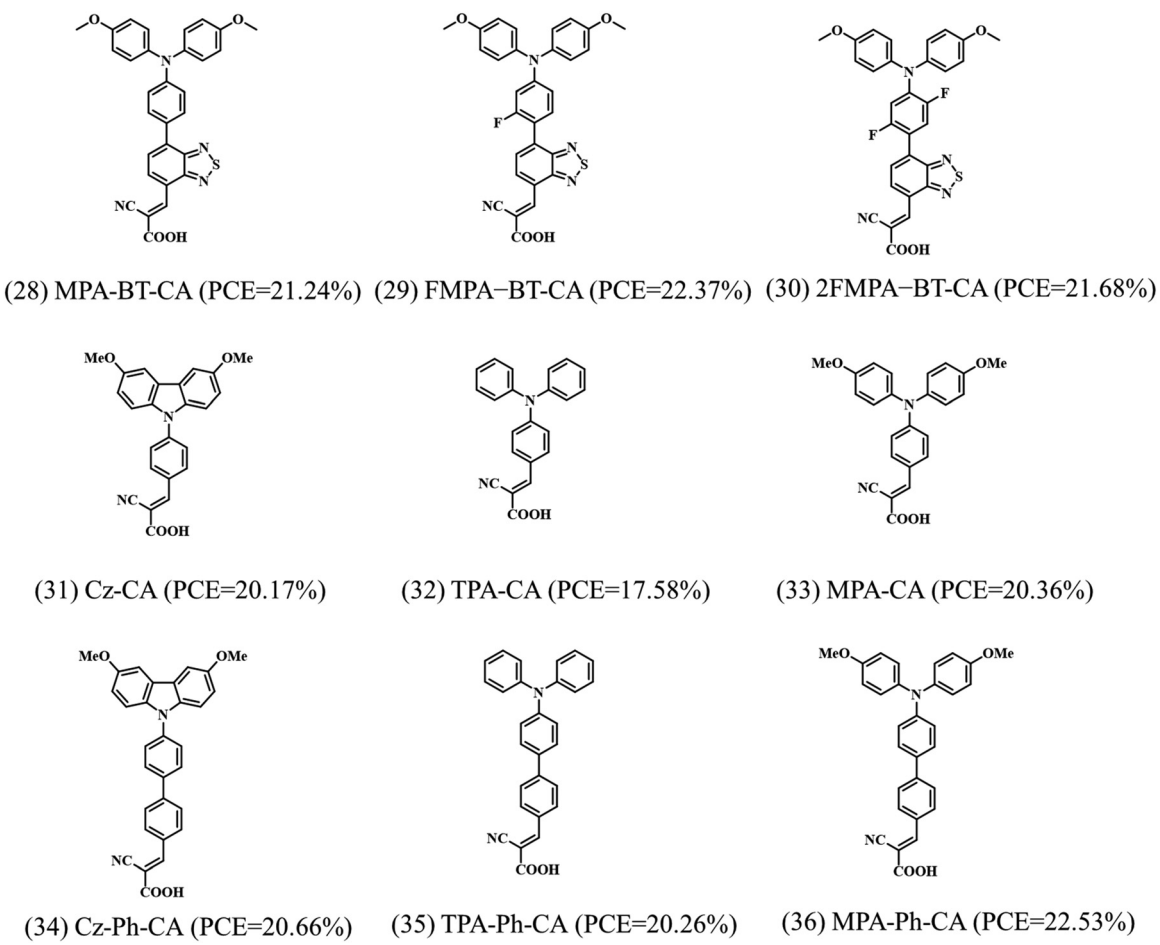

Fig. 9 Molecular structures of the reported SAMs containing cyanoacrylic acid as anchoring groups and the corresponding PCE when they are used as hole selective electrodes in PSCs.

benzo[*c*][1,2,5]-thiadiazole (BT) as the acceptor unit, and 2-cyanoacrylic acid (CA) as the anchoring group.[44] The tunable energy level and defect passivation capability of MPA-BT-CA lead to a PCE of 21.24% (V_{OC} = 1.13 V, J_{SC} = 22.25 mA cm^{-2}, FF = 84.8%) and excellent long-term and thermal stability in p–i–n PSCs. Later, the same group modified the MPA-BT-CA by introducing a fluorine atom in the molecule (FMPA-BT-CA).[45] The fluorination strategy deepened the HOMO level to −5.45 eV matching the energy level of the perovskite layer and enhancing the molecular dipole moment to 13.4 D (Fig. 10a). FMPA-BT-CA passivates the interfacial defects as well, resulting in an efficient PCE of 22.37% in p–i–n PSC. The spacer in the SAM is also crucial for the stability of the molecule. In this sense, the nonconjugated spacer is not beneficial neither for the stability of the electron-rich functional group in SAM nor for the charge transfer due to the localization of charge. Zhu *et al.* thus designed a series of molecules with conjugated spacers and cyanoacrylic acid anchoring groups named Cz-CA, Cz-Ph-CA, TPA-CA, TPA-Ph-CA, MPA-CA, and MPA-Ph-CA. The conjugated spacers enhance the intrinsic photo- and electrical stability of the molecules.[25] Moreover, the intermolecular donor–acceptor groups stabilize the electron-rich functional group through electron/charge delocalization and energy level modulation, resulting in the suitable energy alignment with the perovskite layer. Therefore, the SAM called MPA-Ph-CA achieved a PCE of 22.53% with excellent long-term stability of over 95% of their

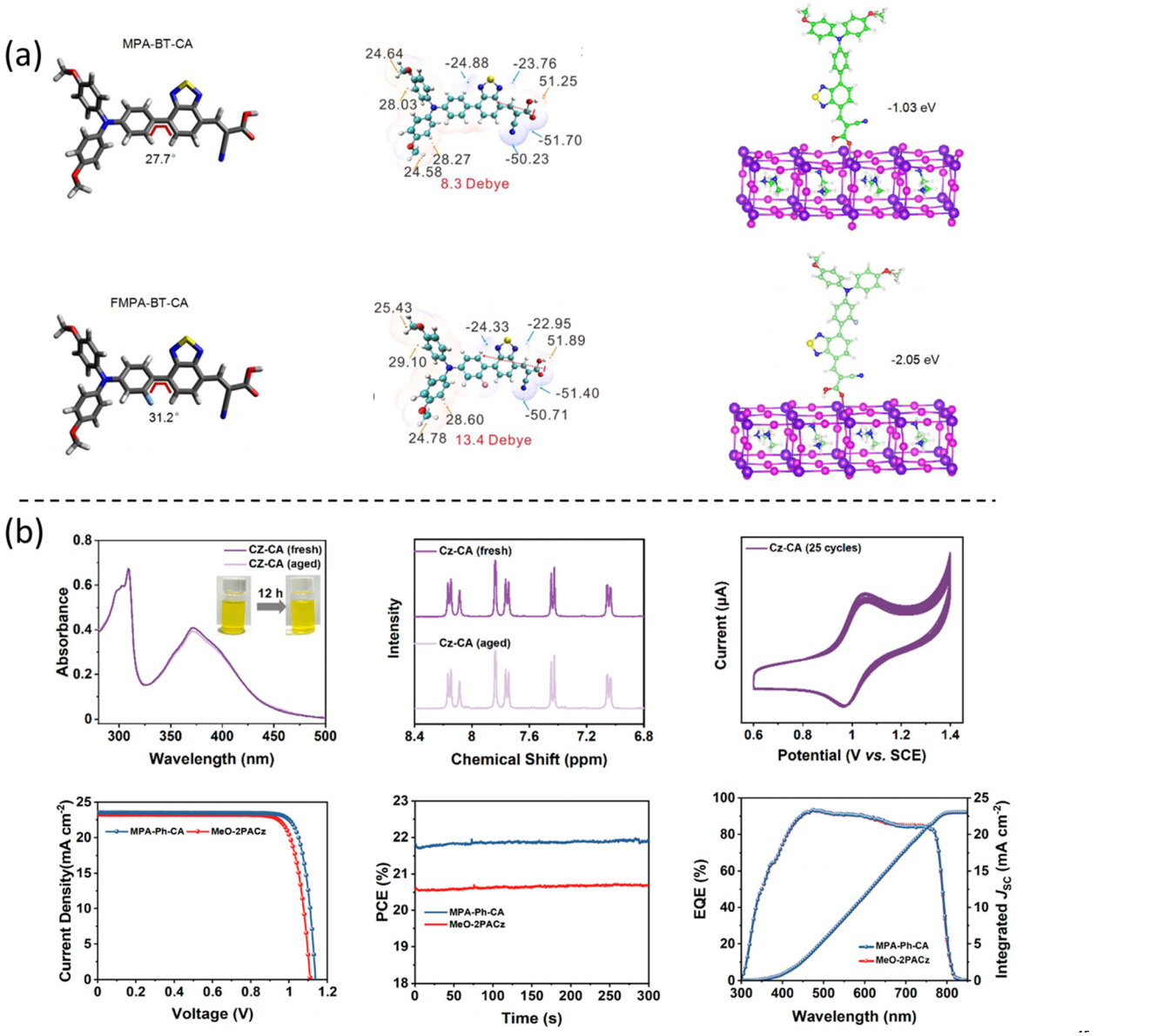

Fig. 10 (a) The calculated dipole moments of the MPA-BT-CA and FMPA-BT-CA SAMs. Reproduced with permission.[45] Copyright 2022, ACS. (b) Measurements to characterize the molecular stability of the CZ-CA SAM and the device performance based on the MPA-Ph-CA molecule. Reproduced with permission.[25] Copyright 2022, ACS.

initial PCE under MPP tracking for 800 h, owing to the high tolerance to UV light of the conjugated SAMs (Fig. 10b).

5. Electron selective SAMs

Compared with the literature related to the hole-selective SAMs, the use of SAMs as the electron selective contacts are less reported, owing to the limited n-type molecules with suitable energy levels for electron transfer and hole-blocking properties. Currently, fullerene-based molecules are mainly used as SAMs with different anchoring groups for electron-selective electrodes in n–i–p PSCs. Petrozza *et al.* reported that self-assembled siloxane-functionalized fullerene molecules could modify FTO, eliminating the need for the traditional TiO_2 layer or any other additional electron-transporting layer, as shown in Fig. 11a.[53] Similar to hole selective SAMs, the fullerene-based SAMs can also be formed in a mild condition process that is easy to scale, with low temperature and low material consumption. The devices reach 15% of stabilized PCE in n–i–p structures. Brabec *et al.* found that a direct surface functionalization of ITO by mixed C_{60}-based SAMs with phosphonic acid as anchoring groups can significantly reduce hysteresis when compared to the TiO_2 electron transport layer (Fig. 11b).[54] The mixed C_{60}-based SAM layer assists the growth of high-quality perovskite films and improves the interfacial charge transfer.

In addition to the fullerene-based electron selective SAMs, other n-type small molecule SAMs have been reported by a few groups, as shown in Fig. 12.[55,56] However, the efficiency is low with these electron-selective SAMs, most probably owing to the mismatching energy alignment to the perovskite layer. Naphthalene diimide (NDI) and perylene diimides (PDI) core-based molecules can lower the LUMO level aligned to the conduction band of perovskite, facilitating electron extraction at the interface. However, the HOMO level of these molecules is not deep enough to effectively block the hole, inducing the interfacial non-radiative recombination when compared to the traditional metal oxide based ESCs. Currently, the PDI-based SAM achieved the highest efficiency of 18.77% with excellent reproducibility and long-term stability.[57] Moreover, Bach *et al.* reported that the chemical and thermal stabilities of the NDI-based SAMs could improve the thermal stability of the devices, reaching T_{80} lifetimes exceeding 800 h for devices at 85 °C in air.[55]

The research about n-type SAMs still lags that of p-type hole selective SAMs. Thus, designing new electron-selective SAMs based on small molecules would be desirable to simplify the fabrication process of n–i–p devices and improve the device performance.

We summarize the SAMs used as electron selective contacts in PSCs, as shown in Table 2 based on p–i–n devices.

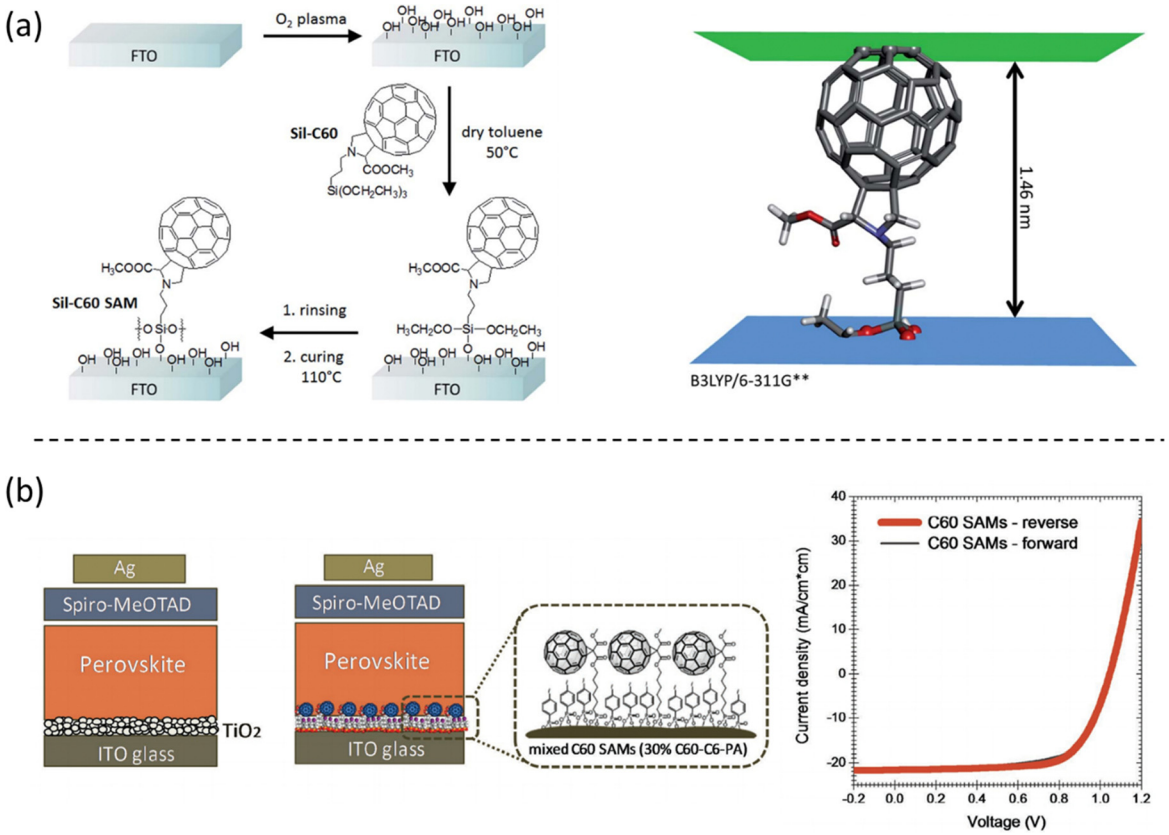

Fig. 11 (a) Illustration of the siloxane-functionalized fullerene self-assembled monolayer fabrication process, and the calculated molecule length. Reproduced with permission.[53] Copyright 2017, RSC. (b) Device structure with fullerene-based SAM electron selective contact and corresponding device performance. Reproduced with permission.[54] Copyright 2017, Wiley.

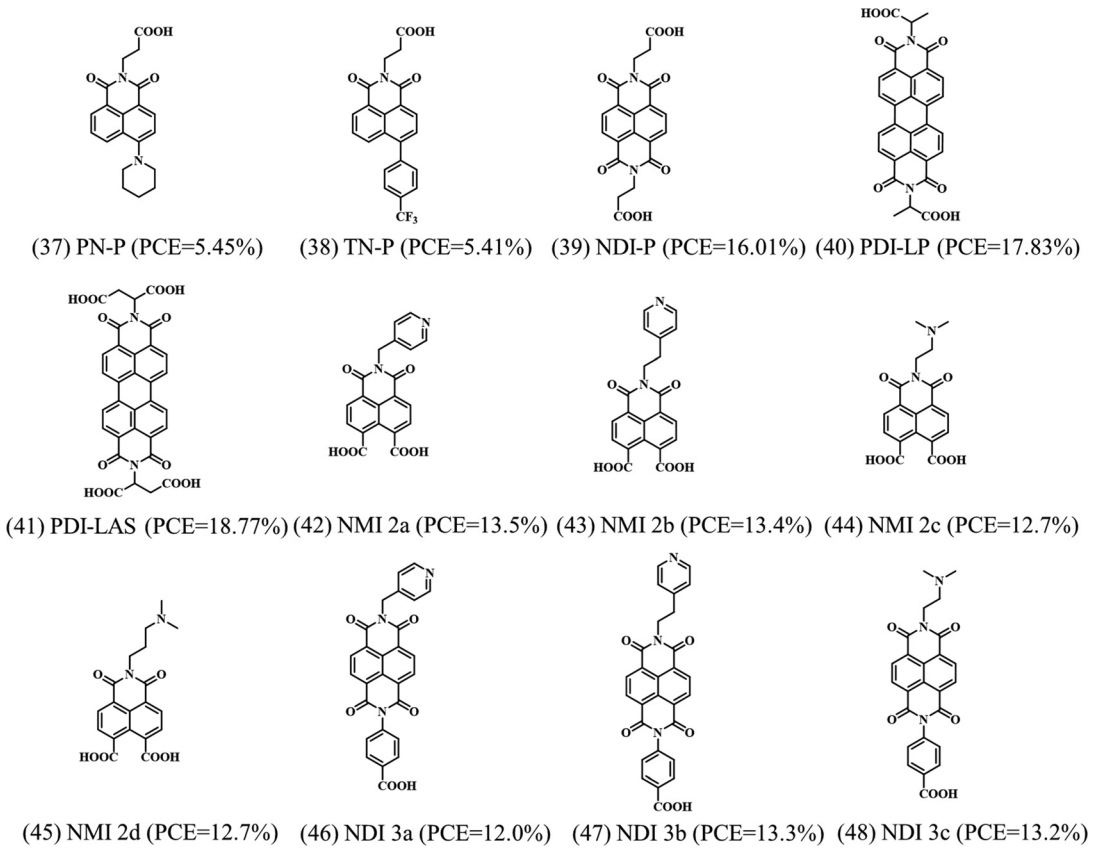

Fig. 12 Molecular structures of the reported non-fullerene small molecule-based electron selective SAMs indicating the PCE achieved when applied in PSCs.

Table 2 The device performance based on electron selective SAMs for n–i–p devices

SAMs	Device configuration	J_{SC} (mA cm^{-2})	V_{OC} (V)	FF (%)	PCE (%)	Ref.
Sil-C60	FTO/Sil-C60/$Cs_{0.05}FA_{0.75}MA_{0.2}PbBr_{0.3}I_{2.7}$/spiro-OMeTAD/Au	19.4	1.04	74	15.2	53
Mix C60 SAM	ITO/30%C60-C6-PA + I-Ph-PA/$MAPbI_3$/spiro-MeOTAD/Ag	21.2	1.05	69	15.4	54
PN-P	ITO/PN-P/$MAPbI_3$/spiro-OMeTAD/Au	10.23	0.76	69.68	5.45	56
TN-P	ITO/TN-P/$MAPbI_3$/spiro-OMeTAD/Au	10.93	0.94	52.94	5.41	56
NDI-P	ITO/NDI-P/$MAPbI_3$/spiro-OMeTAD/Au	20.57	1.05	73.98	16.01	56
PDI-LP	ITO/PDI-LP/$MAPbI_3$/spiro-OMeTAD/Au	22.57	1.08	72.81	17.83	57
PDI-LAS	ITO/PDI-LAS/$MAPbI_3$/spiro-OMeTAD/Au	22.88	1.11	73.98	18.77	57
NMI 2a	ITO/NMI 2a/$Cs_{0.05}FA_{0.8}MA_{0.15}PbI_{2.5}Br_{0.5}$/spiro-OMeTAD/Au	20.0	1.03	62	12.6	55
NMI 2b	ITO/NMI 2b/$Cs_{0.05}FA_{0.8}MA_{0.15}PbI_{2.5}Br_{0.5}$/spiro-OMeTAD/Au	19.7	1.01	62	12.4	55
NMI 2c	ITO/NMI 2c/$Cs_{0.05}FA_{0.8}MA_{0.15}PbI_{2.5}Br_{0.5}$/spiro-OMeTAD/Au	20.4	0.95	57	11.1	55
NMI 2d	ITO/NMI 2d/$Cs_{0.05}FA_{0.8}MA_{0.15}PbI_{2.5}Br_{0.5}$/spiro-OMeTAD/Au	19.8	1.01	60	12.1	55
NDI 3a	ITO/NDI 3a/$Cs_{0.05}FA_{0.8}MA_{0.15}PbI_{2.5}Br_{0.5}$/spiro-OMeTAD/Au	20.5	0.95	54	10.5	55
NDI 3b	ITO/NDI 3b/$Cs_{0.05}FA_{0.8}MA_{0.15}PbI_{2.5}Br_{0.5}$/spiro-OMeTAD/Au	19.6	1.01	62	12.2	55
NDI 3c	ITO/NDI 3c/$Cs_{0.05}FA_{0.8}MA_{0.15}PbI_{2.5}Br_{0.5}$/spiro-OMeTAD/Au	19.8	0.99	56	10.9	55

6. Interfacial charge transfer

The interfacial charge transfer between SAMs and the perovskite film is influenced by the three active functional parts of the SAM which induces additional features not observed in the traditional hole selective contacts (*e.g.* PTAA and PEDOT:PSS). However, its study is limited. Understanding the interfacial charge transfer and the identification of the charge transfer processes are crucial for the further design of novel SAMs that improve the device's performance. As reported by Albrecht *et al.*, MeO-2PACz and 2PACz showed completely different photoluminescence (PL) lifetime decays in the study of the interface between SAM and the perovskite film, although they showed similar device performance.[19] Specifically, MeO-2PACz allows for PL decay times of over 650 ns, while 2PACz has a value of 2 μs. The longer decay time is ascribed to the well defect passivation of buried interfaces by the carbazole groups in 2PACz, lowering the interfacial defect density. Therefore, the passivation effect of SAMs on buried surfaces

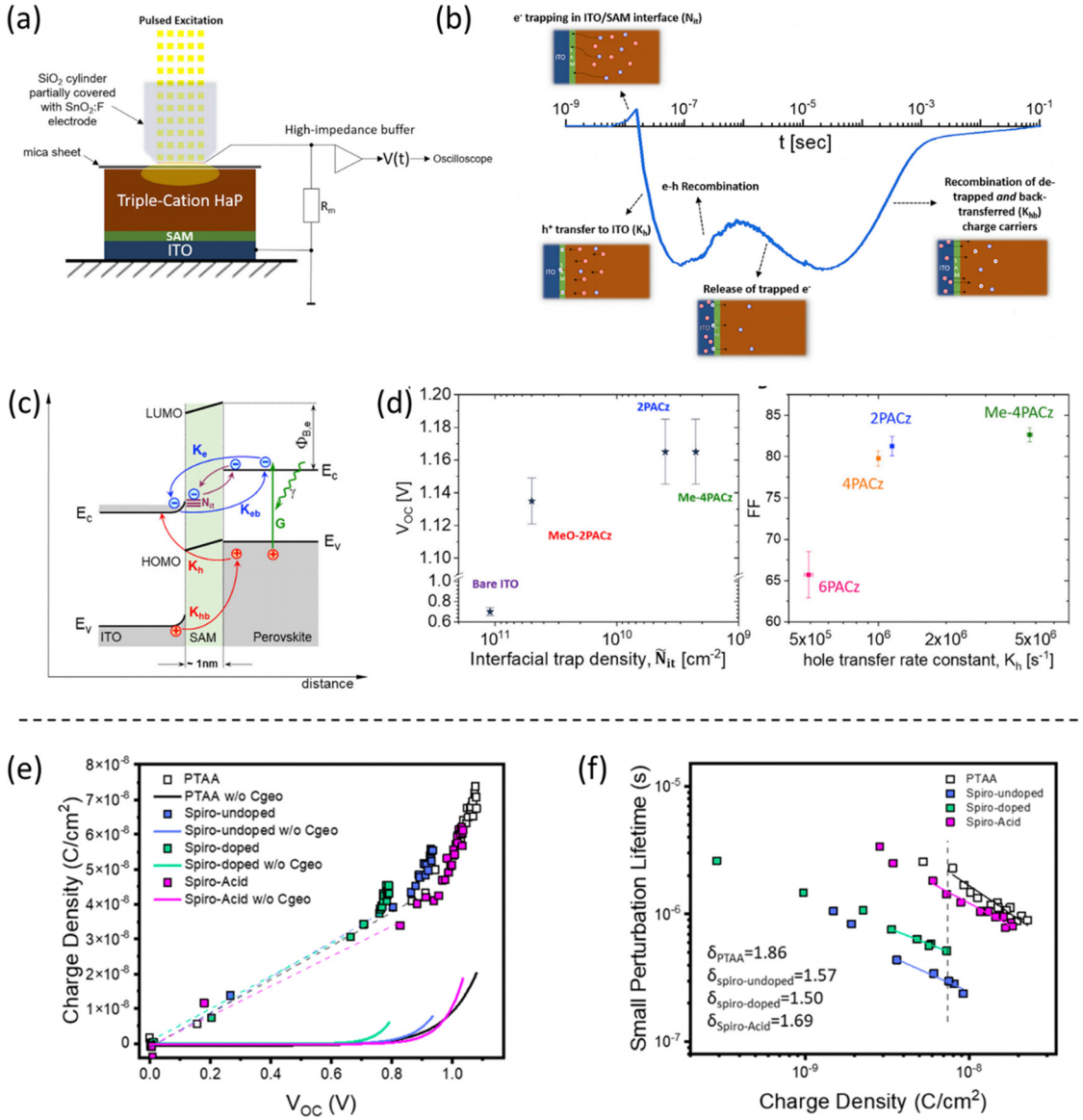

Fig. 13 (a) Schematic description of the SPV measurement setup. (b) The different phenomena occurring at the ITO/SAM/perovskite interface are seen by SPV transients over a wide time range. (c) Illustration of the photoinduced charge transfer dynamics. (d) V_{OC} *versus* the density of interface traps and FF *versus* the hole transfer rate constant of different PACz-based SAM-based PSCs. Reproduced with permission.[22] Copyright 2021, Elsevier. (e) and (f) Charge density as a function of voltage and charge lifetime as a function of charge density under operando conditions for devices made with spiro acid SAM. Reproduced with permission.[34] Copyright 2023, ACS.

of perovskite can be further improved through the molecular design strategy.

The effect of SAMs on the defect passivation of the perovskite buried surface has been further supported by transient surface photovoltage (SPV), which is proposed by Levine and coworkers, as shown in Fig. 13a and b.[22] The SPV technique allows us to analyze the differences in the quality and selectivity of the passivation, together with the hole transfer rate depending on the structure of the SAMs. Unlike measurements of the transient photoluminescence (TrPL), the SPV measurements track the change in the surface potential upon photoexcitation allowing to determine the direction of charge separation, precisely understanding the charge carrier dynamics in a specific interface over a wide time domain, from the generation of the electron–hole pairs to their separation in space and the different electron–hole recombination paths. The analysis of the results of the SPV with a minimalistic kinetic model shows that the structure of SAMs has significant effects on the concentration of defects at the interface. For example, Me-4PACz provided the fastest hole transfer rate constant (4.7×10^6 s^{-1}) and the lower density of interfacial electron traps ($\sim 2 \times 10^9$ cm^{-2}), as shown in Fig. 13c and d, when compared to similar 2PACz, 4PACz, 6PACz or MeO-2PACz.

In addition to the analysis of interfacial charge transfer based on film level, it is also crucial to study the interfaces under operando condition at the device level. Our group has

studied the interfacial charge recombination kinetics comparing spiro-acid SAM and PTAA-based devices, using advanced transient techniques, such as charge extraction (CE), transient photovoltage (TPV), and transient photo-current (TPC) under operando conditions.[34] The spiro-acid-based devices showed faster recombination lifetimes than PTAA-based devices under the same charge density, probably resulting from the unsuitable energy alignment between spiro-acid and perovskite layer, as shown in Fig. 13e and f.

7. Conclusion and perspectives

SAMs have recently emerged as promising molecules to act as selective contacts for high-performance PSCs with low material consumption. Understanding the function of each part of the SAM, including the anchoring group, spacer and functional group, is essential for the molecule design to facilitate interfacial charge transfer, modify the work function of the electrode and grow high-quality perovskite crystals. Unfortunately, there are few works focused on the fundamental research on the role and function of each of the parts of the molecule, all of them based on SPV or transient photoelectronic techniques. More advanced characterization is necessary to deepen the understanding of interfacial reaction and charge transfer dynamics, such as solid-state nuclear magnetic resonance (NMR) and impedance spectroscopy (IS). The combination of theoretical modelling, SPV, transient absorption, solid-state NMR, Kelvin probe force microscopy and IS are powerful and fundamental techniques that would improve the characterization of the interfacial charge transfer and reaction between SAMs and perovskite. Moreover, the coverage of SAMs on the substrate, which is important to confirm the morphology of the SAMs, is rarely reported. Electrochemical and microscopic techniques, such as cyclic voltammetry (CV), high-angle annular dark-field (HAADF) scanning transmission electron microscopy (STEM) and high-resolution transmission electron microscopy (TEM), are powerful tools to calculate or visualize the molecules covered on the substrates. Hence, studies of surface coverage will contribute to unveil the mechanism of the formation of the self-assembled molecular film and its influence in the growth of the perovskites.

In this review, we have analyzed the application of SAMs in efficient PSCs giving suggestions for the design of hole-selective SAMs. First, among various anchoring groups, carboxylic acid and phosphonic acid interact with the substrate creating strong bonds that are responsible for the formation of uniform layers and of large dipoles able to modify the work function of substrate. In addition, the phosphonic acid anchoring group can passivate the buried interfaces to increase the charge extraction rate. Second, both non-conjugated alkyl chains and conjugated spacers can be used to design SAMs for high-performance devices. The spacer can modulate the energy level and the dipole moment of the molecule that affects the work function of the substrate. The selection of the spacer should be systematically considered in combination with the anchoring group and the functional group to balance the charge distribution of the molecule. Finally, the carbazole, triphenylamine and phenoxazine derivatives are commonly used functional groups with strong electron-donating nature that facilitates the charge extraction and transfer. Fine tuning of the functional group with appropriate substituents such as methoxy or methyl molecules or halogen atoms is a useful method to modulate the molecular dipole and induce high quality perovskite films.

Currently, most of the studies focus on p-type SAMs for p–i–n devices, whereas there are very few n-type SAMs for the preparation of n–i–p devices. Therefore, the design and synthesis of n-type small molecule SAMs is necessary to further extend the application of SAMs in PSCs. Similar with the hole selective SAMs, phosphonic acid is an excellent candidate to be used as the anchoring group. As for the electron-accepting group, naphthalene-imide has shown promising results as the functional group in charge of the electron extraction and transfer.

Furthermore, an all SAM-based PSCs made with SAMs in both the hole selective contact and the electron selective contact will be desirable to reduce the non-radiative recombination at top and bottom interfaces, as well as enhance the device stability.

Conflicts of interest

The authors declare that they have no conflict of interest.

Acknowledgements

This work is supported from Spanish Government and AGAUR (PID2019-109389RB-I00, and 2021 SGR 01261, respectively). We also acknowledge the Severo Ochoa Grant MCIN/AEI/10.13039/501100011033 (CEX2019-000925-S) and the project PID2022-139866NB-I00 funded by MCIN/AEI/10.13039/501100011033/FEDER, UE. WL thanks the European Union (Horizon 2020 Marie Skłodowska-Curie COFUND grant agreement No 801474). E.P. also acknowledges ICIQ, CERCA, and ICREA for financial support.

References

1 National Renewable Energy Laboratory, Best research-cell efficiencies chart (2023).
2 Y. Zhao, F. Ma, Z. Qu, S. Yu, T. Shen, H. X. Deng, X. Chu, X. Peng, Y. Yuan, X. Zhang and J. You, Inactive $(PbI_2)_2RbCl$ Stabilizes Perovskite Films for Efficient Solar Cells, *Science*, 1979, **377**(6605), 531–534, DOI: **10.1126/science.abp8873**.
3 J. Park, J. Kim, H.-S. Yun, M. J. Paik, E. Noh, H. J. Mun, M. G. Kim, T. J. Shin and S. I. Seok, Controlled Growth of Perovskite Layers with Volatile Alkylammonium Chlorides, *Nature*, 2023, **616**, 724–730, DOI: **10.1038/s41586-023-05825-y**.
4 S. De Wolf, J. Holovsky, S. J. Moon, P. Löper, B. Niesen, M. Ledinsky, F. J. Haug, J. H. Yum and C. Ballif,

Organometallic Halide Perovskites: Sharp Optical Absorption Edge and Its Relation to Photovoltaic Performance, *J. Phys. Chem. Lett.*, 2014, **5**(6), 1035–1039, DOI: **10.1021/jz500279b**.

5 X. Yang, Y. Fu, R. Su, Y. Zheng, Y. Zhang, W. Yang, M. Yu, P. Chen, Y. Wang, J. Wu, D. Luo, Y. Tu, L. Zhao, Q. Gong and R. Zhu, Superior Carrier Lifetimes Exceeding 6 Ms in Polycrystalline Halide Perovskites, *Adv. Mater.*, 2020, **32**(39), 2002585, DOI: **10.1002/adma.202002585**.

6 K. Galkowski, A. Mitioglu, A. Miyata, P. Plochocka, O. Portugall, G. E. Eperon, J. T. W. Wang, T. Stergiopoulos, S. D. Stranks, H. J. Snaith and R. J. Nicholas, Determination of the Exciton Binding Energy and Effective Masses for Methylammonium and Formamidinium Lead Tri-Halide Perovskite Semiconductors, *Energy Environ. Sci.*, 2016, **9**(3), 962–970, DOI: **10.1039/c5ee03435c**.

7 J. P. Correa-Baena, A. Abate, M. Saliba, W. Tress, T. Jesper Jacobsson, M. Grätzel and A. Hagfeldt, The Rapid Evolution of Highly Efficient Perovskite Solar Cells, *Energy Environ. Sci.*, 2017, **10**(3), 710–727, DOI: **10.1039/c6ee03397k**.

8 H. Min, D. Y. Lee, J. Kim, G. Kim, K. S. Lee, J. Kim, M. J. Paik, Y. K. Kim, K. S. Kim, M. G. Kim, T. J. Shin and S. Il Seok, Perovskite Solar Cells with Atomically Coherent Interlayers on SnO2 Electrodes, *Nature*, 2021, **598**(7881), 444–450, DOI: **10.1038/s41586-021-03964-8**.

9 Z. Zhu, K. Mao, K. Zhang, W. Peng, J. Zhang, H. Meng, S. Cheng, T. Li, H. Lin, Q. Chen, X. Wu and J. Xu, Correlating the Perovskite/Polymer Multi-Mode Reactions with Deep-Level Traps in Perovskite Solar Cells, *Joule*, 2022, **6**(12), 2849–2868, DOI: **10.1016/j.joule.2022.10.007**.

10 M. Degani, Q. An, M. Albaladejo-Siguan, Y. J. Hofstetter, C. Cho, F. Paulus, G. Grancini and Y. Vaynzof, 23.7% Efficient Inverted Perovskite Solar Cells by Dual Interfacial Modification, *Sci. Adv.*, 2023, **7**(49), eabj7930, DOI: **10.1126/sciadv.abj7930**.

11 S. Chen, X. Dai, S. Xu, H. Jiao, L. Zhao and J. Huang, Stabilizing Perovskite-Substrate Interfaces for High-Performance Perovskite Modules, *Science*, 1979, **373**(6557), 902–907, DOI: **10.1126/science.abi6323**.

12 Z. Li, B. Li, X. Wu, S. A. Sheppard, S. Zhang, D. Gao, N. J. Long and Z. Zhu, Organometallic-Functionalized Interfaces for Highly Efficient Inverted Perovskite Solar Cells, *Science*, 1979, **376**(6591), 416–420, DOI: **10.1126/science.abm8566**.

13 C. Bi, Q. Wang, Y. Shao, Y. Yuan, Z. Xiao and J. Huang, Non-Wetting Surface-Driven High-Aspect-Ratio Crystalline Grain Growth for Efficient Hybrid Perovskite Solar Cells, *Nat. Commun.*, 2015, **6**, 7747, DOI: **10.1038/ncomms8747**.

14 J. J. Yoo, G. Seo, M. R. Chua, T. G. Park, Y. Lu, F. Rotermund, Y. K. Kim, C. S. Moon, N. J. Jeon, J. P. Correa-Baena, V. Bulović, S. S. Shin, M. G. Bawendi and J. Seo, Efficient Perovskite Solar Cells *via* Improved Carrier Management, *Nature*, 2021, **590**(7847), 587–593, DOI: **10.1038/s41586-021-03285-w**.

15 S. Zhang, F. Ye, X. Wang, R. Chen, H. Zhang, L. Zhan, X. Jiang, Y. Li, X. Ji, S. Liu, M. Yu, F. Yu, Y. Zhang, R. Wu, Z. Liu, Z. Ning, D. Neher, L. Han, Y. Lin, H. Tian, W. Chen, M. Stolterfoht, L. Zhang, W.-H. Zhu and Y. Wu, Minimizing Buried Interfacial Defects for Efficient Inverted Perovskite Solar Cells, *Science*, 1979, **380**(6643), 404–409, DOI: **10.1126/science.adg3755**.

16 Y. Wang, L. Duan, M. Zhang, Z. Hameiri, X. Liu, Y. Bai and X. Hao, PTAA as Efficient Hole Transport Materials in Perovskite Solar Cells: A Review, *Sol. RRL*, 2022, 2200234, DOI: **10.1002/solr.202200234**.

17 F. M. Rombach, S. A. Haque and T. J. Macdonald, Lessons Learned from Spiro-OMeTAD and PTAA in Perovskite Solar Cells, *Energy Environ. Sci.*, 2021, 5161–5190, DOI: **10.1039/d1ee02095a**.

18 A. Magomedov, A. Al-Ashouri, E. Kasparavičius, S. Strazdaite, G. Niaura, M. Jošt, T. Malinauskas, S. Albrecht and V. Getautis, Self-Assembled Hole Transporting Monolayer for Highly Efficient Perovskite Solar Cells, *Adv. Energy Mater.*, 2018, **8**(32), 1801892, DOI: **10.1002/aenm.201801892**.

19 A. Al-Ashouri, A. Magomedov, M. Roß, M. Jošt, M. Talaikis, G. Chistiakova, T. Bertram, J. A. Márquez, E. Köhnen, E. Kasparavičius, S. Levcenco, L. Gil-Escrig, C. J. Hages, R. Schlatmann, B. Rech, T. Malinauskas, T. Unold, C. A. Kaufmann, L. Korte, G. Niaura, V. Getautis and S. Albrecht, Conformal Monolayer Contacts with Lossless Interfaces for Perovskite Single Junction and Monolithic Tandem Solar Cells, *Energy Environ. Sci.*, 2019, **12**(11), 3356–3369, DOI: **10.1039/c9ee02268f**.

20 S. Y. Kim, S. J. Cho, S. E. Byeon, X. He and H. J. Yoon, Self-Assembled Monolayers as Interface Engineering Nanomaterials in Perovskite Solar Cells, *Adv. Energy Mater.*, 2020, 2002606, DOI: **10.1002/aenm.202002606**.

21 F. Ali, C. Roldán-Carmona, M. Sohail and M. K. Nazeeruddin, Applications of Self-Assembled Monolayers for Perovskite Solar Cells Interface Engineering to Address Efficiency and Stability, *Adv. Energy Mater.*, 2020, 2002989, DOI: **10.1002/aenm.202002989**.

22 I. Levine, A. Al-Ashouri, A. Musiienko, H. Hempel, A. Magomedov, A. Drevilkauskaite, V. Getautis, D. Menzel, K. Hinrichs, T. Unold, S. Albrecht and T. Dittrich, Charge Transfer Rates and Electron Trapping at Buried Interfaces of Perovskite Solar Cells, *Joule*, 2021, **5**(11), 2915–2933, DOI: **10.1016/j.joule.2021.07.016**.

23 S. A. Paniagua, A. J. Giordano, O. L. Smith, S. Barlow, H. Li, N. R. Armstrong, J. E. Pemberton, J. L. Brédas, D. Ginger and S. R. Marder, Phosphonic Acids for Interfacial Engineering of Transparent Conductive Oxides, *Chem. Rev.*, 2016, 7117–7158, DOI: **10.1021/acs.chemrev.6b00061**.

24 E. Aktas, N. Phung, H. Köbler, D. A. González, M. Méndez, I. Kafedjiska, S. H. Turren-Cruz, R. Wenisch, I. Lauermann, A. Abate and E. Palomares, Understanding the Perovskite/Self-Assembled Selective Contact Interface for Ultra-Stable and Highly Efficient p-i-n Perovskite Solar Cells, *Energy Environ. Sci.*, 2021, **14**(7), 3976–3985, DOI: **10.1039/d0ee03807e**.

25 S. Zhang, R. Wu, C. Mu, Y. Wang, L. Han, Y. Wu and W. H. Zhu, Conjugated Self-Assembled Monolayer as Stable

Hole-Selective Contact for Inverted Perovskite Solar Cells, *ACS Mater. Lett.*, 2022, **4**(10), 1976–1983, DOI: **10.1021/acsmaterialslett.2c00799**.

26 A. Al-Ashouri, E. Köhnen, B. Li, A. Magomedov, H. Hempel, P. Caprioglio, J. A. Márquez, A. B. M. Vilches, E. Kasparavicius, J. A. Smith, N. Phung, D. Menzel, M. Grischek, L. Kegelmann, D. Skroblin, C. Gollwitzer, T. Malinauskas, M. Jošt, G. Matič, B. Rech, R. Schlatmann, M. Topič, L. Korte, A. Abate, B. Stannowski, D. Neher, M. Stolterfoht, T. Unold, V. Getautis and S. Albrecht, Monolithic Perovskite/Silicon Tandem Solar Cell with >29% Efficiency by Enhanced Hole Extraction, *Science*, 1979, **370**(6522), 1300–1309, DOI: **10.1126/science.abd4016**.

27 W. Jiang, F. Li, M. Li, F. Qi, F. R. Lin and A. K. Y. Jen, π-Expanded Carbazoles as Hole-Selective Self-Assembled Monolayers for High-Performance Perovskite Solar Cells, *Angew. Chem., Int. Ed.*, 2022, **61**(51), e202213560, DOI: **10.1002/anie.202213560**.

28 K. Choi, H. Choi, J. Min, T. Kim, D. Kim, S. Y. Son, G. W. Kim, J. Choi and T. Park, A Short Review on Interface Engineering of Perovskite Solar Cells: A Self-Assembled Monolayer and Its Roles, *Sol. RRL*, 2020, 1900251, DOI: **10.1002/solr.201900251**.

29 E. Yalcin, M. Can, C. Rodriguez-Seco, E. Aktas, R. Pudi, W. Cambarau, S. Demic and E. Palomares, Semiconductor Self-Assembled Monolayers as Selective Contacts for Efficient PiN Perovskite Solar Cells, *Energy Environ. Sci.*, 2019, **12**(1), 230–237, DOI: **10.1039/c8ee01831f**.

30 E. J. Cassella, E. L. K. Spooner, T. Thornber, M. E. O'Kane, T. E. Catley, J. E. Bishop, J. A. Smith, O. S. Game and D. G. Lidzey, Gas-Assisted Spray Coating of Perovskite Solar Cells Incorporating Sprayed Self-Assembled Monolayers, *Adv. Sci.*, 2022, **9**(14), 2104848, DOI: **10.1002/advs.202104848**.

31 J. Li, J. Dagar, O. Shargaieva, M. A. Flatken, H. Köbler, M. Fenske, C. Schultz, B. Stegemann, J. Just, D. M. Többens, A. Abate, R. Munir and E. Unger, 20.8% Slot-Die Coated MAPbI3 Perovskite Solar Cells by Optimal DMSO-Content and Age of 2-ME Based Precursor Inks, *Adv. Energy Mater.*, 2021, **11**(10), 2003460, DOI: **10.1002/aenm.202003460**.

32 A. Farag, T. Feeney, I. M. Hossain, F. Schackmar, P. Fassl, K. Küster, R. Bäuerle, M. A. Ruiz-Preciado, M. Hentschel, D. B. Ritzer, A. Diercks, Y. Li, B. A. Nejand, F. Laufer, R. Singh, U. Starke and U. W. Paetzold, Evaporated Self-Assembled Monolayer Hole Transport Layers: Lossless Interfaces in p-i-n Perovskite Solar Cells, *Adv. Energy Mater.*, 2023, **13**(8), 2203982, DOI: **10.1002/aenm.202203982**.

33 E. Aktas, R. Pudi, N. Phung, R. Wenisch, L. Gregori, D. Meggiolaro, M. A. Flatken, F. De Angelis, I. Lauermann, A. Abate and E. Palomares, Role of Terminal Group Position in Triphenylamine-Based Self-Assembled Hole-Selective Molecules in Perovskite Solar Cells, *ACS Appl. Mater. Interfaces*, 2022, **14**(15), 17461–17469, DOI: **10.1021/acsami.2c01981**.

34 W. Li, M. Cariello, M. Méndez, G. Cooke and E. Palomares, Self-Assembled Molecules for Hole-Selective Electrodes in Highly Stable and Efficient Inverted Perovskite Solar Cells with Ultralow Energy Loss, *ACS Appl. Energy Mater.*, 2023, **6**(3), 1239–1247, DOI: **10.1021/acsaem.2c02880**.

35 E. Li, C. Liu, H. Lin, X. Xu, S. Liu, S. Zhang, M. Yu, X. M. Cao, Y. Wu and W. H. Zhu, Bonding Strength Regulates Anchoring-Based Self-Assembly Monolayers for Efficient and Stable Perovskite Solar Cells, *Adv. Funct. Mater.*, 2021, **31**(35), 2103847, DOI: **10.1002/adfm.202103847**.

36 A. Ullah, K. H. Park, H. D. Nguyen, Y. Siddique, S. F. A. Shah, H. Tran, S. Park, S. I. Lee, K. K. Lee, C. H. Han, K. Kim, S. J. Ahn, I. Jeong, Y. S. Park and S. Hong, Novel Phenothiazine-Based Self-Assembled Monolayer as a Hole Selective Contact for Highly Efficient and Stable p-i-n Perovskite Solar Cells, *Adv. Energy Mater.*, 2022, **12**(2), 2103175, DOI: **10.1002/aenm.202103175**.

37 A. Ullah, K. H. Park, Y. W. Lee, S. Park, A. B. Faheem, H. D. Nguyen, Y. Siddique, K. K. Lee, Y. Jo, C. H. Han, S. J. Ahn, I. Jeong, S. Cho, B. S. Kim, Y. S. Park and S. Hong, Versatile Hole Selective Molecules Containing a Series of Heteroatoms as Self-Assembled Monolayers for Efficient p-i-n Perovskite and Organic Solar Cells, *Adv. Funct. Mater.*, 2022, **32**(49), 2208793, DOI: **10.1002/adfm.202208793**.

38 Z. Li, Q. Tan, G. Chen, H. Gao, J. Wang, X. Zhang, J. Xiu, W. Chen and Z. He, Simple and Robust Phenoxazine Phosphonic Acid Molecules as Self-Assembled Hole Selective Contacts for High-Performance Inverted Perovskite Solar Cells, *Nanoscale*, 2022, **15**(4), 1676–1686, DOI: **10.1039/d2nr05677a**.

39 X. Deng, F. Qi, F. Li, S. Wu, F. R. Lin, Z. Zhang, Z. Guan, Z. Yang, C. S. Lee and A. K. Y. Jen, Co-Assembled Monolayers as Hole-Selective Contact for High-Performance Inverted Perovskite Solar Cells with Optimized Recombination Loss and Long-Term Stability, *Angew. Chem., Int. Ed.*, 2022, **61**(30), e202203088, DOI: **10.1002/anie.202203088**.

40 W. Wang, X. Liu, J. Wang, C. Chen, J. Yu, D. Zhao and W. Tang, Versatile Self-Assembled Molecule Enables High-Efficiency Wide-Bandgap Perovskite Solar Cells and Organic Solar Cells, *Adv. Energy Mater.*, 2023, **13**, 2300694, DOI: **10.1002/aenm.202300694**.

41 R. Guo, X. Zhang, X. Zheng, L. Li, M. Li, Y. Zhao, S. Zhang, L. Luo, S. You, W. Li, Z. Gong, R. Huang, Y. Cui, Y. Rong, H. Zeng and X. Li, Tailoring Multifunctional Self-Assembled Hole Transporting Molecules for Highly Efficient and Stable Inverted Perovskite Solar Cells, *Adv. Funct. Mater.*, 2023, **33**(10), 2211955, DOI: **10.1002/adfm.202211955**.

42 M. A. Truong, T. Funasaki, L. Ueberricke, W. Nojo, R. Murdey, T. Yamada, S. Hu, A. Akatsuka, N. Sekiguchi, S. Hira, L. Xie, T. Nakamura, N. Shioya, D. Kan, Y. Tsuji, S. Iikubo, H. Yoshida, Y. Shimakawa, T. Hasegawa, Y. Kanemitsu, T. Suzuki and A. Wakamiya, Tripodal Triazatruxene Derivative as a Face-On Oriented Hole-Collecting Monolayer for Efficient and Stable Inverted Perovskite Solar Cells, *J. Am. Chem. Soc.*, 2023, **145**(13), 7528–7539, DOI: **10.1021/jacs.3c00805**.

43 Q. Tan, Z. Li, G. Luo, X. Zhang, B. Che, G. Chen, H. Gao, D. He, G. Ma, J. Wang, J. Xiu, H. Yi, T. Chen and Z. He, Inverted Perovskite Solar Cells Using Dimethylacridine-

Based Dopants, *Nature*, 2023, **620**, 545–551, DOI: **10.1038/s41586-023-06207-0**.

44 Y. Wang, Q. Liao, J. Chen, W. Huang, X. Zhuang, Y. Tang, B. Li, X. Yao, X. Feng, X. Zhang, M. Su, Z. He, T. J. Marks, A. Facchetti and X. Guo, Teaching an Old Anchoring Group New Tricks: Enabling Low-Cost, Eco-Friendly Hole-Transporting Materials for Efficient and Stable Perovskite Solar Cells, *J. Am. Chem. Soc.*, 2020, **142**(39), 16632–16643, DOI: **10.1021/jacs.0c06373**.

45 Q. Liao, Y. Wang, M. Hao, B. Li, K. Yang, X. Ji, Z. Wang, K. Wang, W. Chi, X. Guo and W. Huang, Green-Solvent-Processable Low-Cost Fluorinated Hole Contacts with Optimized Buried Interface for Highly Efficient Perovskite Solar Cells, *ACS Appl. Mater. Interfaces*, 2022, **14**(38), 43547–43557, DOI: **10.1021/acsami.2c10758**.

46 T. Bauer, T. Schmaltz, T. Lenz, M. Halik, B. Meyer and T. Clark, Phosphonate- and Carboxylate-Based Self-Assembled Monolayers for Organic Devices: A Theoretical Study of Surface Binding on Aluminum Oxide with Experimental Support, *ACS Appl. Mater. Interfaces*, 2013, **5**(13), 6073–6080, DOI: **10.1021/am4008374**.

47 L. Li, Y. Wang, X. Wang, R. Lin, X. Luo, Z. Liu, K. Zhou, S. Xiong, Q. Bao, G. Chen, Y. Tian, Y. Deng, K. Xiao, J. Wu, M. I. Saidaminov, H. Lin, C. Q. Ma, Z. Zhao, Y. Wu, L. Zhang and H. Tan, Flexible All-Perovskite Tandem Solar Cells Approaching 25% Efficiency with Molecule-Bridged Hole-Selective Contact, *Nat. Energy*, 2022, **7**(8), 708–717, DOI: **10.1038/s41560-022-01045-2**.

48 X. Zheng, Z. Li, Y. Zhang, M. Chen, T. Liu, C. Xiao, D. Gao, J. B. Patel, D. Kuciauskas, A. Magomedov, R. A. Scheidt, X. Wang, S. P. Harvey, Z. Dai, C. Zhang, D. Morales, H. Pruett, B. M. Wieliczka, A. R. Kirmani, N. P. Padture, K. R. Graham, Y. Yan, M. K. Nazeeruddin, M. D. McGehee, Z. Zhu and J. M. Luther, Co-Deposition of Hole-Selective Contact and Absorber for Improving the Processability of Perovskite Solar Cells, *Nat. Energy*, 2023, **8**, 462–472, DOI: **10.1038/s41560-023-01227-6**.

49 J. Wang, K. Liu, L. Ma and X. Zhan, Triarylamine: Versatile Platform for Organic, Dye-Sensitized, and Perovskite Solar Cells, *Chem. Rev.*, 2016, 14675–14725, DOI: **10.1021/acs.chemrev.6b00432**.

50 L. Zhang and J. M. Cole, Anchoring Groups for Dye-Sensitized Solar Cells, *ACS Appl. Mater. Interfaces*, 2015, 3427–3455, DOI: **10.1021/am507334m**.

51 A. B. Muñoz-García, I. Benesperi, G. Boschloo, J. J. Concepcion, J. H. Delcamp, E. A. Gibson, G. J. Meyer, M. Pavone, H. Pettersson, A. Hagfeldt and M. Freitag, Dye-Sensitized Solar Cells Strike Back, *Chem. Soc. Rev.*, 2021, 12450–12550, DOI: **10.1039/d0cs01336f**.

52 X. Li, C. C. Chen, M. Cai, X. Hua, F. Xie, X. Liu, J. Hua, Y. T. Long, H. Tian and L. Han, Efficient Passivation of Hybrid Perovskite Solar Cells Using Organic Dyes with COOH Functional Group, *Adv. Energy Mater.*, 2018, **8**(20), 1800715, DOI: **10.1002/aenm.201800715**.

53 P. Topolovsek, F. Lamberti, T. Gatti, A. Cito, J. M. Ball, E. Menna, C. Gadermaier and A. Petrozza, Functionalization of Transparent Conductive Oxide Electrode for TiO2-Free Perovskite Solar Cells, *J. Mater. Chem. A Mater.*, 2017, **5**(23), 11882–11893, DOI: **10.1039/c7ta02405c**.

54 Y. Hou, S. Scheiner, X. Tang, N. Gasparini, M. Richter, N. Li, P. Schweizer, S. Chen, H. Chen, C. O. R. Quiroz, X. Du, G. J. Matt, A. Osvet, E. Spiecker, R. H. Fink, A. Hirsch, M. Halik and C. J. Brabec, Suppression of Hysteresis Effects in Organohalide Perovskite Solar Cells, *Adv. Mater. Interfaces*, 2017, **4**(11), 1700007, DOI: **10.1002/admi.201700007**.

55 S. O. Fürer, K. J. Rietwyk, F. Pulvirenti, D. P. McMeekin, M. A. Surmiak, S. R. Raga, W. Mao, X. Lin, Y. Hora, J. Wang, Y. Shi, S. Barlow, D. S. Ginger, S. R. Marder and U. Bach, Naphthalene-Imide Self-Assembled Monolayers as a Surface Modification of ITO for Improved Thermal Stability of Perovskite Solar Cells, *ACS Appl. Energy Mater.*, 2023, **6**(2), 667–677, DOI: **10.1021/acsaem.2c02735**.

56 L. Li, Y. Wu, E. Li, C. Shen, H. Zhang, X. Xu, G. Wu, M. Cai and W. H. Zhu, Self-Assembled Naphthalimide Derivatives as an Efficient and Low-Cost Electron Extraction Layer for n-i-p Perovskite Solar Cells, *Chem. Commun.*, 2019, **55**(88), 13239–13242, DOI: **10.1039/c9cc06345e**.

57 F. Ye, D. Zhang, X. Xu, H. Guo, S. Liu, S. Zhang, Y. Wu and W. H. Zhu, Anchorable Perylene Diimides as Chemically Inert Electron Transport Layer for Efficient and Stable Perovskite Solar Cells with High Reproducibility, *Sol. RRL*, 2021, **5**(3), 2000736, DOI: **10.1002/solr.202000736**.